Response and fluctuations of a two-state signaling module with feedback

Manoj Gopalakrishnan,* Peter Borowski,† Frank Jülicher, and Martin Zapotocky

Max Planck Institute for the Physics of Complex Systems, Nöthnitzer Straße 38, 01187 Dresden, Germany
(Received 4 July 2006; revised manuscript received 16 April 2007; published 7 August 2007)

We study the stochastic kinetics of a signaling module consisting of a two-state stochastic point process with negative feedback. In the active state, a product is synthesized which increases the active-to-inactive transition rate of the process. We analyze this simple autoregulatory module using a path-integral technique based on the temporal statistics of state flips of the process. We develop a systematic framework to calculate averages, autocorrelations, and response functions by treating the feedback as a weak perturbation. Explicit analytical results are obtained to first order in the feedback strength. Monte Carlo simulations are performed to test the analytical results in the weak feedback limit and to investigate the strong feedback regime. We conclude by relating some of our results to experimental observations in the olfactory and visual sensory systems.

I. INTRODUCTION

Signal transduction in biological cells refers to the set of processes by which the cells receive and process information from the environment. From the realization of the extracellular stimulus to its final recognition by the cell or organism, there is, in general, a complex biochemical reaction network, commonly referred to as the signal transduction pathway. Faithful transmission of information through the pathway may require amplification and adaptation, which is often accomplished through positive (amplification) and negative (adaptation) feedback mechanisms built into the reaction network.

External and intrinsic noise can potentially limit the faithful transduction of a "signal" (information encoded in the intensity of the external stimulus and its spatiotemporal variation) [1,2]. Since cellular biochemical networks often function with a limited number of reacting molecules, noise is always present, and an important question is how the cell physiology maintains its robustness in spite of the randomness in the underlying molecular events [3]. In the context of signal transduction, external noise refers to the randomness in the signal (fluctuations in the local concentration of the extracellular ligand, etc.), whereas intrinsic noise is a collective effect produced by the inherent stochasticity of the transduction mechanisms itself, such as random opening and closing of the ion channels, fluctuations in reaction rates, and so on [4–11]. Although randomness and noise are beneficial in some instances (population heterogeneity being a well-known example [12]), by and large, cells have evolved the means to control biochemical noise through regulatory mechanisms (such as negative feedback) to ensure the robustness of biochemical networks [13]. Indeed, in the context of electrical circuits, negative feedback is a well-known noise-reduction mechanism used in devices such as amplifiers and oscillators (see [14] for a review and important references).

Complex signaling pathways can often be productively viewed as consisting of recurring *modules* [15,16]. A module is typically made up of multiple species of interacting molecules acting together with a specific function. A signal transduction pathway may thus be described in terms of a series of modules, interacting with each other [17]. In very general terms, a module receives a signal (from the extracellular environment, or from another module) and transmits it, possibly in a different form (e.g., chemical signals converted to electrical pulses). Each module can function to a certain extent in isolation, but interaction among modules and their coordination are crucial for carrying out all the complex functions of the cell.

In this paper, we analyze a signaling module based on a single protein that switches between active (A*) and inactive (A) states. In the active state, a certain molecular species C is produced with a fixed rate. The accumulation of C increases the A* → A transition rate (Fig. 1), leading to negative feedback on the production of C. In addition, C is removed at a fixed rate independent of the activation state. As an example, Fig. 2 illustrates the modularity of signal transduction and the occurrence of the module defined in Fig. 1, for the specific case of vertebrate olfactory sensory neurons (reviewed in [18,19]). (A closely related pathway also operates in cone photoreceptors in the retina.)
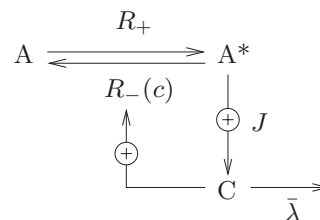

FIG. 1. The simple two-component autoregulatory signaling module with negative feedback studied in this paper. The product C (with concentration c), generated with rate J in the active state A*, enhances the deactivation rate R_-. C is removed with a rate $\bar{\lambda}$ independent of the activation state of A. An input signal encoded in a temporal change $R_+(t)$ is transduced into an output signal $c(t)$.

*Present address: Harish-Chandra Research Institute, Chhatnag Road, Jhunsi, Allahabad 211019 India; manoj@mri.ernet.in

†Present address: Department of Mathematics, The University of British Columbia, 1984 Mathematics Road, Vancouver, BC V6T 1Z2, Canada.
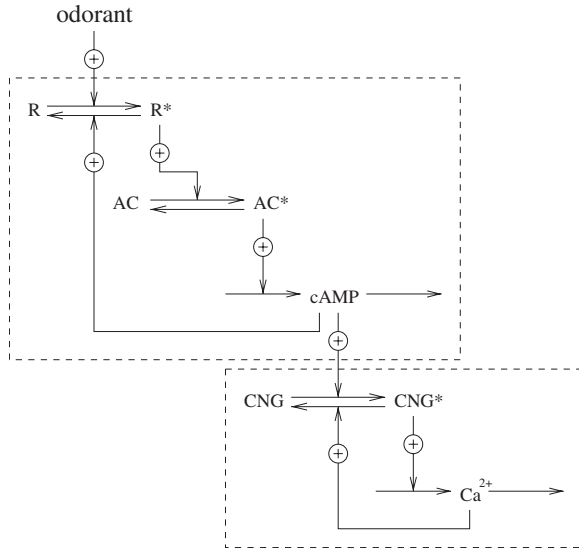
FIG. 2. A schematic representation of the modularity of signal transduction in olfactory sensory neurons. (The arrows with a + sign indicate enhancement of the reaction rates; arrows without signs indicate the direction of the reactions in the conventional sense.) After binding of an odorant (external stimulus) to the receptor R, the enzyme adenylate cyclase (AC) is activated and produces the "second messenger" cAMP, leading in turn to the opening of cyclic-nucleotide-gated (CNG) ion channels and to the depolarization of the cell membrane. Two negative feedback mechanisms (reviewed in [23]) are shown in the figure: (i) cAMP-activated kinase phosphorylates (and therefore deactivates) the receptor R, and (ii) Ca^{2+} ions bound to calmodulin inhibit the Ca^{2+} channels, which is crucial for adaptation to repeated odorant stimuli [24,25]. The signal transduction pathway can be viewed as consisting of two modules of the type shown in Fig. 1, connected in series.

In the work presented, we develop a systematic analytical framework to study the dynamics of the simple autoregulatory module shown in Fig. 1. Without the feedback, the activation and deactivation kinetics would be described by a two-state Poisson process. In the presence of feedback, the deactivation rate, at any given time, becomes dependent on the history of transitions, and makes the effective two-state kinetics non-Markovian. We use a path-integral technique to evaluate the effects of feedback perturbatively, which enables us to derive the noise from the dynamics of the system. This is in contrast to stochastic analysis of biochemical networks based on Langevin equations [20] with additive white noise (see, e.g., [17,21]).

We obtain explicit analytical expressions for the different statistical averages as well as correlation and response functions of the module in the limit of weak feedback. We also perform Monte Carlo simulations to test the analytical results in the weak feedback limit and to investigate the strong feedback regime. The path-integral formalism we develop is similar to the one described in [22], and the system considered is the same as in [9]. The calculations in [9], however, focus on steady state probability distributions rather than temporal correlations.

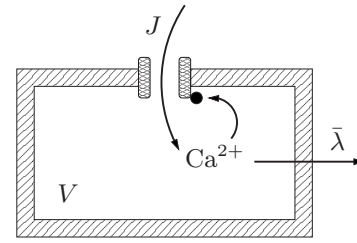The paper is arranged into four sections. Section II provides a brief description of our simple model of a stochastic signaling module with feedback. All important quantities are introduced and the notation is defined. In Sec. III, we present and develop the path-integral formalism. In Sec. IV, we compute the different Green's functions using this formalism to first order in feedback strength. Section V is devoted to the calculation of the averages and correlation functions, and Sec. VI contains the calculation of the response functions. Section VII presents the results of Monte Carlo simulations and their comparison to analytical results. Our conclusions and outlook for further extensions are presented in Sec. VIII. Four appendices detail some of the analytical calculations.

FIG. 3. A channel in the open state permits the entry of ions (rate *J*) into a small compartment of volume *V*. The ions, once inside, increase the closing rate of the channel, and are also removed from the compartment at a constant rate $\bar{\lambda}$.

II. TWO-STATE MODEL: GENERAL SETUP

We describe our model of a two-state signaling module using the example of an ion channel connected to a small cellular compartment (Fig. 3). The channel on the cell membrane exists in one of two conformational states: *open*, when the ions enter through the channel, and *closed* when this is not allowed. The state of the channel at time *t* is represented by $S(t)$, with $S=1$ being the open state and $S=0$, the closed state. The $0 \rightarrow 1$ transition takes place with a rate R_+, and the reverse transition $1 \rightarrow 0$ occurs with a rate R_-. Let us denote by $\bar{c}(\bar{t})$, the ion (which in the case of the olfactory signaling pathway is Ca^{2+}) concentration inside the compartment at time $\bar{t}$. The kinetics of $\bar{c}$ is described by the equation

$$\frac{d\bar{c}}{d\bar{t}} = \frac{J}{V}S(\bar{t}) - \bar{\lambda}\bar{c}(\bar{t}). \qquad (1)$$

In the above equation, *J* represents the molar current of ions entering the cell through the channel in the open state, $\bar{\lambda}$ represents the total rate of removal of ions by membrane pumps, and *V* is the volume of the compartment. The channel kinetics is specified by the opening rate R_+ and closing rate R_-. We assume the existence of a negative feedback corresponding to a rate R_- that increases with increasing ion concentration. If the effect of the feedback is weak, one may expand to linear order and write

$$R_-(\bar{c}) \approx R_-^0 + \bar{\alpha}\bar{c}(\bar{t}), \qquad (2)$$

where R_-^0 is the closing rate of the channel when no ions are present in the compartment and the coupling parameter $\bar{\alpha}$ specifies the feedback strength. We further assume that, in
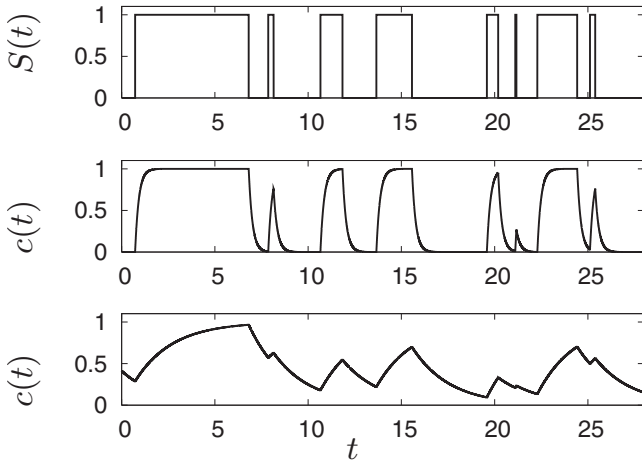
FIG. 4. The figure illustrates the kinetics of channel openings and Ca^{2+} concentration for two typical runs, with $r_+ = 0.5$ and $\lambda = 5$ (top and middle) and $\lambda = 0.5$ (top and bottom) in the absence of feedback ($\alpha = 0$). Note that for larger λ, $c(t)$ almost follows the steplike kinetics of $S(t)$.

general, an external signal is received by the module as a change in the opening rate (due, e.g., to the binding of extracellular ligands to the channel). We may write

$$R_+(\bar{\phi}) = R_+^0 + \bar{\phi}(\bar{t}), \qquad (3)$$

where R_+^0 is the intrinsic opening rate of the channel in the absence of external stimulus, and $\bar{\phi}(\bar{t})$ defines the stimulus. Eqs. (1)–(3) specify the dynamics of the problem.

It is now convenient to adopt a dimensionless formulation of the problem. The inverse of the intrinsic closing rate R_-^0 is chosen as the unit of time and the ratio $J/(\bar{\lambda}V)$ (i.e., the maximum achievable ion concentration) is the unit of $\bar{c}$. Using these two quantities, we scale all the other parameters, and the complete list of dimensionless parameters is then as follows:

$$c = \frac{\bar{\lambda}V}{J}\bar{c}, \quad \alpha = \frac{\bar{\alpha}J/V}{\bar{\lambda}R_-^0}, \quad \lambda = \frac{\bar{\lambda}}{R_-^0}, \quad \phi = \frac{\bar{\phi}}{R_-^0},$$

$$r_+ = \frac{R_+}{R_-^0}, \quad r_- = \frac{R_-}{R_-^0} = 1 + \alpha c, \quad t = R_-^0 \bar{t}. \qquad (4)$$

The dynamical equation for $c(t)$ is then simplified to $\frac{dc}{dt} = \lambda[S(t) - c(t)]$, with the solution

$$c(t) = \lambda \int_{-\infty}^{t} e^{-\lambda(t-t')} S(t') dt'. \qquad (5)$$

Figure 4 shows two typical time evolution curves of $S(t)$ and $c(t)$. Note, from Eq. (5), that in the limit $\lambda \to \infty$, $c(t) \approx S(t)$, which is illustrated in Fig. 4. In this limit, the Ca^{2+} is drained from the compartment as soon as the channel closes, and consequently, the time evolution of $c(t)$ closely follows the channel state. In this sense, λ is an important control parameter in our model, and determines how much the dynamic characteristics of $c(t)$ (including fluctuations and response

functions) are tied to the corresponding quantities for the channel state. These aspects will be discussed more in Sec. V and later.

The combined set of Eqs. (1)–(3) describe the kinetics of $S(t)$, which may be characterized using, for instance, the n-point functions ($n=1,2,\cdots$): $\langle S(t_0)\dots S(t_{n-1})\rangle$. The corresponding functions for $c(t)$ are then easily computed from these using Eq. (5) as follows:

$$\langle c(t_0) \cdots c(t_{n-1}) \rangle = \lambda^n e^{-\lambda(t_0 + \cdots + t_{n-1})}$$

$$\times \int_{-\infty}^{t_0} dt_0' \cdots \int_{-\infty}^{t_{n-1}} dt_{n-1}' e^{\lambda(t_0' + \cdots + t_{n-1}')}$$

$$\times \langle S(t_0') \cdots S(t_{n-1}') \rangle. \qquad (6)$$

The angular brackets $\langle \cdots \rangle$ represent statistical averaging over the different temporal histories of the process. In particular, when the external signal is time independent, the system reaches a steady state, where the one-point functions $\langle S \rangle$ and $\langle c \rangle$ are constants, while the autocorrelation and crosscorrelation functions

$$\mathcal{C}_S(t) = \lim_{t_0 \to \infty} \langle S(t_0)S(t_0 + t) \rangle - \langle S \rangle^2,$$

$$\mathcal{C}_c(t) = \lim_{t_0 \to \infty} \langle c(t_0)c(t_0 + t) \rangle - \langle c \rangle^2,$$

$$\mathcal{C}_{Sc}(t) = \lim_{t_0 \to \infty} \langle S(t_0)c(t_0 + t) \rangle - \langle S \rangle \langle c \rangle, \qquad (7)$$

are stationary in time. In particular, it also follows from Eq. (5) that

$$\langle c \rangle = \langle S \rangle \qquad (8)$$

in the steady state. We may also define the power spectral densities for the fluctuations in S and c from the stationary autocorrelation functions, for example,

$$P_c(\omega) = 2 \int_0^{\infty} \mathcal{C}_c(t) \cos(\omega t) dt = \frac{\lambda^2}{\lambda^2 + \omega^2} P_S(\omega), \qquad (9)$$

where the relation between P_c and P_S follows from Eq. (5). Note that for $\omega \ll \lambda$, $P_c \simeq P_S$, whereas when $\omega \gg \lambda$, $P_c \sim \omega^{-2} P_S$. This has an interesting physical interpretation: when λ is small over the time scales of interest, Ca^{2+} kinetics is slow, and this effectively suppresses the power-spectrum at larger frequencies compared to the case of large λ.

The response of the system to a time-dependent external perturbation $\phi(t)$ is $\langle S(t) \rangle^\phi - \langle S \rangle$ and $\langle c(t) \rangle^\phi - \langle c \rangle$, where the superscript ϕ indicates that the function needs to be evaluated in the presence of the perturbation. When the external signal is weak, i.e., $\phi(t) \ll r_+$, the response is characterized using the linear response functions $\chi_S(t)$ and $\chi_c(t)$ defined through the following relations:

$$\chi_S(t) = \frac{d}{dt} \lim_{\phi \to 0} \frac{1}{\phi} (\langle S \rangle^\phi - \langle S \rangle),$$

$$\chi_c(t) = \frac{d}{dt} \lim_{\phi \to 0} \frac{1}{\phi}(\langle c \rangle^\phi - \langle c \rangle). \tag{10}$$

Using Eq. (5), the following relation between the response functions is also easily proved:

$$\chi_c(t) = \lambda \int_0^t \chi_S(t') e^{-\lambda(t-t')} dt'. \tag{11}$$

In the following sections, we present explicit calculations of the correlation and linear response functions of the model in the presence of feedback. Most of the specific results in this paper are derived for a constant r_+.

III. PATH-INTEGRAL FORMULATION

We start by introducing the propagator $\Pi_{ij}(t_0, c_0; t, c)$ with $i, j = \{0, 1\}$ that gives the probability density to find $S(t) = j$ and $c(t) = c$ given that $S(t_0) = i$ and $c(t_0) = c_0$. The mean open fraction of the channel in steady state can be written as

$$\langle S \rangle = \int_0^1 \Pi_{i1}(-\infty, c_0; 0, c) dc, \tag{12}$$

and is independent of i and c_0. We define two different mean values of the concentration c, namely, the mean concentrations during periods when the channel is closed and open, respectively, starting from a special initial state $S(t=0)=0$, $c(t=0)=0$ as follows:

$$\langle c(t) \rangle_0 = \int_0^1 \Pi_{i0}(0, 0; t, c) c \, dc,$$

$$\langle c(t) \rangle_1 = \int_0^1 \Pi_{i1}(0, 0; t, c) c \, dc. \tag{13}$$

The autocorrelation function of S in steady state is

$$\langle S(0)S(t) \rangle = \int_0^1 dc \int_0^1 dc_1 \Pi_{i1}(-\infty, c_0; 0, c_1) \Pi_{11}(0, c_1; t, c). \tag{14}$$

The linear response function can be written using a step function $r_+ \to r_+ + \phi(t)$ [with $\phi(t) = \phi_0 \theta(t)$, where $\theta(t)$ is the Heaviside function] as a stimulus, as follows:

$$\chi_S(t) = \frac{\partial}{\partial t} \frac{\partial}{\partial \phi_0} \bigg|_{\phi_0 = 0} \sum_j \int_0^1 dc \int_0^1 dc_1 \Pi_{ij}(-\infty, c_0; 0, c_1)$$

$$\times \Pi_{j1}^{\phi_0}(0, c_1; t, c). \tag{15}$$

In order to formulate a path-integral representation of the propagator, we define the functional $\mathcal{P}_{ij}[t_0, t; \{\tau_k\}_{k=1}^N; c_0; N]$ of $S(t)$ with $t > t_0$. It represents the probability that a certain time evolution of the system from $S(t_0) = i$ and $c(t_0) = c_0$ to $S(t) = j$ is realized. This time evolution is characterized by the set of times $\{\tau_k\}_{k=1}^N$ at which the state switches from $S=0$ to 1 or from $S=1$ to 0. The number N represents the total number of such state changes in the time interval $[t_0, t]$ and is even if

$i=j$ and odd otherwise. The propagator $\Pi_{ij}(t_0, c_0; t, c)$ can be expressed as a sum over all possible realizations of $S(t)$ as

$$\Pi_{ij}(t_0, c_0; t, c) = \sum_N \int \mathcal{D}\tau \mathcal{P}_{ij}[t_0, t; \{\tau_k\}_{k=1}^N; c_0; N] \delta[c(t) - c],$$
$$\tag{16}$$

where $\int \mathcal{D}\tau \equiv \int_{t_0}^t d\tau_1 \int_{\tau_1}^t d\tau_2 \cdots \int_{\tau_{N-1}}^t d\tau_N$.

It is convenient to introduce the reduced propagator or Green's function

$$G_{ij}(t_0, c_0; t) \equiv \int_0^1 \Pi_{ij}(t_0, c_0; t, c) dc, \tag{17}$$

which can be written as

$$G_{ij}(t_0, c_0; t) = \sum_N \int \mathcal{D}\tau \mathcal{P}_{ij}[t_0, t; \{\tau_k\}_{k=1}^N; c_0; N]. \tag{18}$$

By definition the following relations hold:

$$G_{01} + G_{00} = 1 = G_{10} + G_{11}. \tag{19}$$

Note that in the absence of feedback, the functionals $\mathcal{P}_{01}$ and $\mathcal{P}_{11}$ do not depend on c, and the history dependence is thus absent. In this case, the expression for the n-point functions reduces to the product of Green's functions: $\langle S(t_0) \cdots S(t_{n-1}) \rangle = G_{01}^{(0)}(-\infty, t_0) G_{11}^{(0)}(t_0, t_1) \cdots G_{11}^{(0)}(t_{n-2}, t_{n-1})$, where the superscript (0) denotes the absence of feedback (valid for the rest of the paper and all quantities) [26]. As special cases, the one- and two-point functions in the absence of feedback are given by

$$\langle S(t_0) \rangle = \langle S \rangle = G_{01}^{(0)}(-\infty, t_0),$$

$$\langle S(t_0)S(t) \rangle = G_{01}^{(0)}(-\infty, t_0) G_{11}^{(0)}(t_0, t), \tag{20}$$

when $\alpha = 0$.

We now write down the functionals $\mathcal{P}_{ij}$ in the explicit form. The expressions are presented only for $\mathcal{P}_{00}$; extensions to the other cases are straightforward. Furthermore, since the different Green's functions are related [Eq. (19) and Eq. (37) later], it is enough to compute one of them. It is instructive to start with $\alpha = 0$, where the transitions $0 \to 1$ and $1 \to 0$ are characterized by the (time-invariant) rates r_+ and $r_- = r_-^0 \equiv 1$, respectively (in terms of scaled time). Let us consider a certain history of the process such that the channel is closed at $t=0$ and t, but changes state an even number N times in between, at times $\tau_1, \tau_2, \ldots, \tau_N$. First consider the interval $[0, \tau_1]$. The probability that the channel remains in state 0 until time τ_1 has the form $P_0(0, \tau_1) = e^{-r_+ \tau_1}$. Similarly, the probability of the channel to remain in state 1 during the time interval $[\tau_1, \tau_2]$ is $P_1(\tau_1, \tau_2) = e^{-(\tau_2 - \tau_1)}$. The (differential) probability for the whole process is

$$\mathcal{P}_{00}^{(0)}[0, t; \{\tau_i\}_{i=1}^N; N] d\tau_1 d\tau_2 \cdots d\tau_N = r_+^{N/2}$$

$$\times \prod_{i=1}^N d\tau_i P_0(0, \tau_1) P_1(\tau_1, \tau_2) P_0(\tau_2, \tau_3) \cdots P_0(\tau_N, t). \tag{21}$$
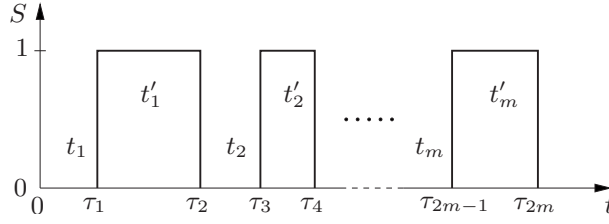
FIG. 5. A schematic diagram of time evolution of $S(t)$, showing the time flip-variables τ_i versus the interval variables t_i and t_i'.

We now substitute for P_0 and P_1, and make the transformation from flip times $\{\tau_i\}_{i=1}^N$ to time-interval variables $\{t_j, t_j'\}_{j=1}^m$ with $m=N/2$, where the $\{t_j\}$ denote the times when the channel is closed and the $\{t_j'\}$ when it is open (see Fig. 5). The relation between the flip times and the time intervals is summarized below:

$$\tau_1 = t_1,$$

$$\tau_i = \sum_{l=1}^{i/2} t_l + \sum_{l=1}^{i/2} t_l' \quad \text{even} \quad i \geqslant 2,$$

$$\tau_j = \sum_{l=1}^{(j+1)/2} t_l + \sum_{l=1}^{(j-1)/2} t_l' \quad \text{odd} \quad j > 1. \tag{22}$$

The Jacobian for the transformation is $J=1$, as follows from Eq. (22). The probability functional thus has the form

$$\mathcal{P}_{00}^{(0)}[0,t;\{t_i\},\{t_i'\};2m] = r_+^m e^{-F_{00}(0,t;\{t_i'\};m)}, \tag{23}$$

with the weight factor F_{00} given by

$$F_{00}(0,t;\{t_i'\};m) = r_+ t + (1-r_+)\sum_{i=1}^m t_i'. \tag{24}$$

In the presence of the feedback coupling to $c(t)$, the expression for $\mathcal{P}_{00}$ is modified to

$$\mathcal{P}_{00}[0,t;\{t_i\},\{t_i'\};c_0;2m] = r_+^m \prod_{i=2}^{2m} {}'[1+\alpha c(\tau_i)]$$
$$\times e^{-F_{00} - \alpha \sum_{j=1}^{\prime\prime 2m-1} \int_{\tau_j}^{\tau_{j+1}} d\tau c(\tau)}, \tag{25}$$

where the prime (double prime) on the product or sum symbol indicates that the running index is always even (odd). The above expression may be expanded in powers of the dimensionless feedback strength α as follows:

$$\mathcal{P}_{00}[0,t;\{t_i\},\{t_i'\};c_0;2m] = r_+^m e^{-F_{00}}\left[1 + \alpha\left(\sum_{i=2}^{2m}{}' c(\tau_i)\right.\right.$$
$$\left.\left. - \sum_{j=1}^{2m-1}{}'' \int_{\tau_j}^{\tau_{j+1}} d\tau c(\tau)\right) \right] + O(\alpha^2). \tag{26}$$

Equation (26) is the basis for more specific and detailed calculations to follow in the next sections.

IV. COMPUTATION OF GREEN'S FUNCTIONS

A. Computation of G_{00}

For instructive purposes, we first show how the Green's function $G_{00}^{(0)}(0,t)$ in the absence of feedback is computed using our formalism. In this case the exact answer is easily found by solving its rate equation

$$\partial_t G_{00}^{(0)} = r_- - (r_- + r_+)G_{00}^{(0)}, \tag{27}$$

with $r_- = r_-^0 = 1$ and the initial condition $G_{00}^{(0)}(0,0) = 1$. The solution is

$$G_{00}^{(0)}(0,t) = \frac{1}{1+r_+}(1 + r_+ e^{-(1+r_+)t}). \tag{28}$$

This Green's function can also be computed using the path-integral technique outlined previously, more specifically from Eq. (18) using Eqs. (23) and (24). For simplicity, let us put $t_0=0$, and define the Laplace transform of the Green's function $\tilde{G}_{00}^{(0)}(s) = \int_0^\infty G_{00}^{(0)}(0,t)e^{-st}dt$. The calculation is most easily done using the generalized convolution theorem presented in Appendix A [Eq. (A1)]. Using this technique, the path integral in Eq. (18) becomes a product in the s space, and the result is

$$\tilde{G}_{00}^{(0)}(s) = g(s + r_+),$$

with

$$g(s) = \frac{1}{s}\sum_{m=0}^\infty \left(\frac{1}{s}\right)^m\left(\frac{r_+}{s+1-r_+}\right)^m. \tag{29}$$

After summing the geometric series in Eq. (29), we find that $\tilde{G}_{00}^{(0)}(s) = (s+1)/[s(s+1+r_+)]$, which, upon inversion, gives Eq. (28).

Let us now extend the previous calculation to include feedback, and compute $G_{00}(0,c_0;t)$ to first order in α:

$$G_{00}(0,c_0;t) = G_{00}^{(0)}(0,t) + \alpha G_{00}^{(1)}(0,c_0;t) + O(\alpha^2). \tag{30}$$

From Eqs. (26) and (18), we find that $G_{00}^{(1)}(0,c_0;t)$ depends only linearly on c_0: $G_{00}^{(1)}(0,c_0;t) = G_{00}^{(1)}(0,c_0=0;t) + c_0 f(t)$. Putting together the c_0 independent terms, we write

$$G_{00}(0,c_0;t) = G_{00}(0,c_0=0;t) + \alpha c_0 f(t) + O(\alpha^2), \tag{31}$$

where $c_0 f(t)$ is simply the $O(\alpha)$ term in $G_{00}(0,c_0;t)$, when the channel evolves in a situation with $J \equiv 0$ so that $r_-(t) = 1 + \alpha c_0 e^{-\lambda t}$. Using this $r_-(t)$, the function $f(t)$ is easily determined by solving the rate equation [Eq. (27)] with the

initial condition $G_{00}(0,c_0;0)=1$. The result is

$$f(t) = \frac{r_+}{\lambda}\left(\frac{-1}{1+r_+-\lambda}e^{-(1+r_+)t} + \frac{1}{1+r_+}e^{-(1+r_++\lambda)t}\right.$$

$$\left. + \frac{\lambda}{(1+r_+)(1+r_+-\lambda)}e^{-\lambda t}\right). \tag{32}$$

The function $G_{00}(0,c_0=0;t)$ itself may be expressed in terms of three integrals as follows:

$$G_{00}(0,c_0=0;t) = e^{-r_+t}\left(1 + \sum_{m=1}^{\infty} r_+^m[I_0(t;m) + \alpha(I_1(t;m)\right.$$

$$\left. - I_2(t;m))]\right) + O(\alpha^2), \tag{33}$$

where

$$I_0(t;m) = \int \mathcal{D}T e^{-(1-r_+)\Sigma_{i=1}^m t_i'},$$

$$I_1(t;m) = \int \mathcal{D}T e^{-(1-r_+)\Sigma_{i=1}^m t_i'}\sum_{i=2}^{2m}{}'c(\tau_i),$$

$$I_2(t;m) = \int \mathcal{D}T e^{-(1-r_+)\Sigma_{i=1}^m t_i'}\sum_{j=1}^{2m-1}{}''\int_{\tau_j}^{\tau_{j+1}} d\tau c(\tau). \tag{34}$$

Note that we have introduced the compact notation $\int \mathcal{D}T \equiv \int_0^t dt_1 \int_0^{t-t_1} dt_1' \int_0^{t-t_1-t_1'} dt_2 \cdots \int_0^{t-\cdots-t_m} dt_m'$ for the integration measure. The explicit calculations are done most conveniently in terms of Laplace-transformed variables, defined in the standard way: $\tilde{f}(s) = \int_0^\infty f(t)e^{-st}dt$. The previous Eq. (33) becomes, in this notation,

$$\tilde{G}_{00}(c_0=0;s) = (s+r_+)^{-1} + \sum_{m=1}^{\infty} r_+^m[\tilde{I}_0(s+r_+;m) + \alpha(\tilde{I}_1(s$$

$$+ r_+;m) - \tilde{I}_2(s+r_+;m))] + O(\alpha^2). \tag{35}$$

The calculation of the integrals $\tilde{I}_0$, $\tilde{I}_1$, and $\tilde{I}_2$ is done in Appendix A. We omit further details, and present only the final result to obtain:

$$G_{00}(0,c_0=0;t) \equiv G_{00}^{(0)}(0,t) + \alpha G_{00}^{(1)}(0,c_0=0;t) = G_{00}^{(0)}(0,t)$$

$$+ \alpha\frac{r_+}{(1+r_+)^2}\left[\frac{r_++\lambda}{1+r_++\lambda} - e^{-\lambda t}\frac{r_+(1+r_+)}{(1+r_+-\lambda)^2}\right.$$

$$- e^{-(1+r_++\lambda)t}\frac{1+r_+}{\lambda(1+r_++\lambda)}$$

$$+ e^{-(1+r_+)t}\left(\frac{(1+r_+)(\lambda-1)t}{1+r_+-\lambda}\right.$$

$$\left.\left. + \frac{r_+^2 - (\lambda-1)^3 + r_+(2-3\lambda+2\lambda^2)}{\lambda(1+r_+-\lambda)^2}\right)\right] + O(\alpha^2). \tag{36}$$

B. Relation between G_{11} and G_{00}

We will now show that there is a nontrivial relation between $G_{11}(0,c_0=0;t)$ and $G_{00}(0,c_0=0;t)$, as follows:

$$G_{11}(0,c_0=0;t) = G_{01}(0,c_0=0;t) + \frac{\partial_t G_{00}(0,c_0=0;t)}{\partial_t G_{00}(0,c_0=0;t)|_{t=0}}, \tag{37}$$

which will be shown to be true up to $O(\alpha)$. To prove this, let us start with the case $\alpha=0$. Then, the following relation is true for any arbitrary $0 \leq t' \leq t$:

$$G_{01}^{(0)}(0,t) = G_{00}^{(0)}(0,t')G_{01}^{(0)}(t',t) + G_{01}^{(0)}(0,t')G_{11}^{(0)}(t',t). \tag{38}$$

Let us now take the limit of $t' \to 0$, and use the Taylor expansions $G_{00}^{(0)}(0,t') = 1 + t'\frac{\partial G_{00}^{(0)}(0,t)}{\partial t}|_{t=0} + \cdots$, $G_{ij}^{(0)}(t',t) = G_{ij}^{(0)}(t-t') = G_{ij}^{(0)}(0,t) - t'\frac{\partial G_{ij}^{(0)}(0,t)}{\partial t} + \cdots$ as well as the condition $G_{01}^{(0)} = 1 - G_{00}^{(0)}$. After substituting these back into Eq. (38), we arrive at Eq. (37).

In the presence of feedback, Eq. (38) is not true anymore because of the explicit history dependence. However, using expansions of the two Green's functions $G_{01}(t',c';t)$ and $G_{11}(t',c';t)$ similar to Eq. (31),

$$G_{01}(t',c';t) = G_{01}(t',c'=0;t) + \alpha c' f_1(t-t') + O(\alpha^2),$$

$$G_{11}(t',c';t) = G_{11}(t',c'=0;t) + \alpha c' f_2(t-t') + O(\alpha^2), \tag{39}$$

Eq. (37) can be shown to be valid also for $\alpha \neq 0$ [to $O(\alpha)$]. The proof as well as the functions $f_1(t)$ and $f_2(t)$ are given in Appendix B.

V. AVERAGES AND CORRELATORS

A. Averages and comparison to mean-field analysis

The mean fraction of open channels in the steady state is now easily found as $\langle S \rangle = \lim_{t\to\infty}[1 - G_{00}(0,c_0=0;t)]$, and the result is

$$\langle S \rangle = \langle c \rangle = \frac{r_+}{1+r_+}\left(1 - \alpha\frac{r_++\lambda}{(1+r_+)(1+r_++\lambda)}\right) + O(\alpha^2). \tag{40}$$

For comparison, we may also compute the same quantity using the mean-field approach. In general, the steady state obeys the relation

$$r_+(1 - \langle S \rangle) = \langle r_- S \rangle = \langle S \rangle + \alpha\langle cS \rangle. \tag{41}$$

In the spirit of mean-field analysis, we now assume that the fluctuations in S and c are independent, $\langle cS \rangle = \langle c \rangle\langle S \rangle$. Making use of the equality $\langle c \rangle = \langle S \rangle$ in Eq. (41) (valid in the steady state), one obtains a quadratic equation for $\langle S \rangle$. The solution is

$$\langle S \rangle_{\mathrm{MF}} = \frac{\sqrt{(1+r_+)^2 + 4\alpha r_+} - (1+r_+)}{2\alpha}. \qquad (42)$$

A small-α expansion of the square root gives

$$\langle S \rangle_{\mathrm{MF}} = \frac{r_+}{1+r_+} - \alpha\frac{r_+^2}{(1+r_+)^3} + O(\alpha^2). \qquad (43)$$

The mean-field treatment can be expected to be valid if the calcium dynamics is slow compared to the channel dynamics, as in this case the calcium concentration exhibits only small fluctuations around its mean value and can be replaced by a constant [as will be seen explicitly in Eq. (52)]. Indeed, the full result in Eq. (40) reduces to the mean-field result in Eq. (43) when $\lambda \ll r_+$ and $\lambda \ll 1$. For all other values of λ, the mean-field analysis underestimates the effect of feedback.

A second limiting case of interest is the situation where the pump rate is large: $\lambda \to \infty$, in which case, from Eq. (5), we find that $c(t) \approx S(t)$ at all times t. In this case the closing rate may be approximated as $r_- \approx 1 + \alpha$ since $c \simeq 1$ in the open state of the channel. The mean open fraction, therefore, is given by

$$\langle S \rangle \simeq \frac{r_+}{1+r_++\alpha} \approx \frac{r_+}{1+r_+} - \alpha\frac{r_+}{(1+r_+)^2} + O(\alpha^2). \quad (44)$$

It is easily verified that this expression is the limit of the one given in Eq. (40) to $O(\alpha)$ for $\lambda \gg r_+$ and $\lambda \gg 1$.

Our perturbative result for the mean fraction of open channels [Eq. (40)] is contained in the results of [9].

B. Autocorrelation functions

To compute the two-point function of S, we put the definition of the reduced propagator [Eq. (17)] into Eq. (14) to obtain:

$$\langle S(0)S(t) \rangle = \int_0^1 dc_1 \Pi_{i1}(-\infty, c_0; 0, c_1) G_{11}(0, c_1; t). \quad (45)$$

Using Eq. (39) together with Eqs. (12) and (13), we arrive at

$$\langle S(0)S(t) \rangle = \langle S \rangle G_{11}(0, c_0 = 0; t) + \alpha\langle c \rangle_1 f_2(t) + O(\alpha^2), \qquad (46)$$

where $G_{11}(0, c_0=0; t)$ is given by Eq. (37), $G_{00}(0, c_0=0; t)$ is given by Eq. (36), $f_2(t)$ is given by Eq. (B1), and $\langle c \rangle_1$ is the steady state value of the restricted average $\langle c(t) \rangle_1$ [Eq. (13)] and calculated in Appendix C. Using Eq. (46) and the steady state average in Eq. (40), we find the autocorrelation function of S [Eq. (7)] to be

$$C_S(t) = \frac{r_+}{(1+r_+)^2}e^{-(1+r_+)t} + \alpha(B_1 e^{-(1+r_+)t} + C_1 e^{-\lambda t} \\ + D_1 e^{-(1+r_++\lambda)t} + E_1 t e^{-(1+r_+)t}) + O(\alpha^2). \qquad (47)$$

The coefficients B_1, C_1, D_1, E_1 are given in Appendix D. We observe that the first order correction term introduces two new time scales. Furthermore, the feedback introduces a term nonmonotonic in time, whose sign depends on the relative

values of λ and r_+. For $\lambda < 1$ and $\lambda > 1+r_+$, $E_1 > 0$, whereas for intermediate values $1 < \lambda < 1+r_+$, $E_1 < 0$. This term is the first indication that the feedback term introduces qualitative differences in the decay of the autocorrelation function.

The corresponding correlator for $c(t)$ is computed from Eq. (6) using the two-point function in Eq. (46). The result is

$$C_c(t) = \frac{r_+\lambda}{(1+r_+)^2[(1+r_+)^2 - \lambda^2]}[e^{-\lambda t}(1+r_+) - \lambda e^{-(1+r_+)t}] \\ + \alpha(B_2 e^{-(1+r_+)t} + C_2 e^{-\lambda t} + D_2 e^{-(1+r_++\lambda)t} + E_2 t e^{-(1+r_+)t} \\ + F_2 t e^{-\lambda t}) + O(\alpha^2). \qquad (48)$$

The coefficients B_2, C_2, D_2, E_2, F_2 are given in Appendix D. Similar to the previous case, the first order correction term has introduced two new time scales, and unlike the previous case, there are two nonmonotonic terms in time. From Eq. (48) and using Eq. (9), we now find the power spectrum for c fluctuations to $O(\alpha)$ as follows:

$$P_c(\omega) = 2\frac{r_+\lambda^2}{(1+r_+)(\omega^2+\lambda^2)[\omega^2+(1+r_+)^2]} \\ + 2\alpha\left(\frac{B_2(1+r_+)}{\omega^2+(1+r_+)^2} + \frac{C_2\lambda}{\omega^2+\lambda^2} + \frac{D_2(1+r_++\lambda)}{\omega^2+(1+r_++\lambda)^2} \\ + \frac{E_2[(1+r_+)^2-\omega^2]}{[(1+r_+)^2+\omega^2]^2} + \frac{F_2(\lambda^2-\omega^2)}{(\lambda^2+\omega^2)^2}\right) + O(\alpha^2). \quad (49)$$

For large ω, $P_c(\omega) \sim \omega^{-4}$, which is true with and without feedback [27]. However, for small frequencies, i.e., $\omega \ll \lambda$ in particular, the power spectrum for c effectively decays as ω^{-2} because large λ attenuates the high frequency (but still less than λ) noise.

From Appendix D, we see that $F_2 < 0$ always, whereas $E_2 < 0$ for $1 < \lambda < 1+r_+$ and $E_2 > 0$ for $\lambda < 1$ and $\lambda > 1+r_+$. The interplay of the time scales λ and $1+r_+$ gives rise to nontrivial time dependence in the autocorrelation function. This results in a variety of possible time courses, examples of which can be observed in numerical simulations presented in Sec. VII.

From the correlators Eqs. (47) and (48), the fluctuations are also determined easily. We define the mean-squared fluctuations through

$$(\delta S)^2 = \langle S^2 \rangle - \langle S \rangle^2 = \langle S \rangle(1 - \langle S \rangle) = C_S(0),$$

$$(\delta c)^2 = \langle c^2 \rangle - \langle c \rangle^2 = C_c(0). \qquad (50)$$

The channel state fluctuation has the following characteristic: Since $(\delta S)^2 = \langle S \rangle(1 - \langle S \rangle)$, its maximum is always $\frac{1}{4}$, which is reached when $\langle S \rangle = \frac{1}{2}$, independent of feedback. The RMS fluctuations, to first order in α are given by

$$\delta S = \frac{\sqrt{r_+}}{1 + r_+}\left(1 - \frac{\alpha}{2}\frac{(1 - r_+)(r_+ + \lambda)}{(1 + r_+)(1 + r_+ + \lambda)}\right) + O(\alpha^2),$$

$$\delta c = \sqrt{\frac{r_+\lambda}{(1 + r_+)^2(1 + r_+ + \lambda)}}\left(1 + \frac{\alpha}{2}\times\frac{r_+^3 + r_+^2(3\lambda - 2) + r_+(2\lambda^2 - 4\lambda - 3) - \lambda(2\lambda + 3)}{(1 + r_+)(1 + r_+ + \lambda)(1 + r_+ + 2\lambda)}\right) + O(\alpha^2). \tag{51}$$

For the channel state, we see that the first order correction term simply reverses sign at the point $r_+ = 1$ (when the intrinsic opening and closing rates are the same). The fluctuations are enhanced by feedback when $r_+ < 1$ and suppressed when $r_+ > 1$.

The calcium fluctuation can likewise be increased or decreased by feedback, depending on the values of λ and r_+. The precision of output of the signaling module is given by the relative fluctuation (normalized standard deviation) in Ca^{2+}. Using Eqs. (40) and (51) we obtain

$$\frac{\delta c}{\langle c\rangle} = \sqrt{\frac{\lambda}{r_+(1 + r_+ + \lambda)}}\left(1 + \alpha\frac{(r_+ + \lambda)(-1 + r_+ + 2\lambda)}{2(1 + r_+ + 2\lambda)(1 + r_+ + \lambda)}\right)$$
$$+ O(\alpha^2). \tag{52}$$

Clearly for $\lambda > \frac{1}{2}$ the relative fluctuation is increased for any value of r_+, while for sufficiently small λ it is increased when r_+ is large and decreased when $r_+ < 1$. The precision of output can thus be improved by feedback when the input is weak (r_+ is small).

VI. RESPONSE FUNCTIONS

A. Computation of χ_S and χ_c

When a step stimulus $r_+ + \phi_0\theta(t)$ is applied to the system, the response function [Eq. (15)] in S can be written using the definition of the Green's function [Eq. (17)] together with Eq. (39), as

$$\chi_S(t) = \frac{\partial}{\partial t}\left.\frac{\partial}{\partial\phi_0}\right|_{\phi_0=0}[\langle S\rangle G_{11}^{\phi_0}(0,0;t) + (1 - \langle S\rangle)G_{01}^{\phi_0}(0,0;t)$$
$$+ \alpha(f_1^{\phi_0}(t)\langle c\rangle_0 + f_2^{\phi_0}(t)\langle c\rangle_1)] + O(\alpha^2), \tag{53}$$

where ϕ_0 appearing as a superscript indicates that r_+ is to be replaced by $r_+ + \phi_0$. Putting in the two Green's functions [Eqs. (36) and (37)] together with Eqs. (B1) and the restricted calcium averages (computed in Appendix C), the final result is

$$\chi_S(t > 0) = \frac{1}{1 + r_+}e^{-(1+r_+)t} + \alpha(B_3 e^{-(1+r_+)t} + C_3 e^{-\lambda t}$$
$$+ D_3 e^{-(1+r_++\lambda)t} + E_3 t e^{-(1+r_+)t}) + O(\alpha^2), \tag{54}$$

where B_3, C_3, D_3, E_3 are given in Appendix D. The coefficient E_3 of the nonmonotonic term is negative for $\lambda < 1$ and $\lambda > 1 + r_+$, and positive for $1 < \lambda < 1 + r_+$. The contribution from these terms makes the decay of the response function faster (relative to $\alpha = 0$) for small and large λ and slower for intermediate λ.

The response function $\chi_c(t)$ is now calculated from Eq. (54) using Eq. (11), yielding to first order in feedback

$$\chi_c(t > 0) = \frac{\lambda}{(1 + r_+)(1 + r_+ - \lambda)}(e^{-\lambda t} - e^{-(1+r_+)t})$$
$$+ \alpha(B_4 e^{-(1+r_+)t} + C_4 e^{-\lambda t} + D_4 e^{-(1+r_++\lambda)t}$$
$$+ E_4 t e^{-(1+r_+)t} + F_4 t e^{-\lambda t}) + O(\alpha^2), \tag{55}$$

where $F_4 < 0$, while $E_4 < 0$ for $\lambda < 1$ and $\lambda > 1 + r_+$ and $E_4 > 0$ for $1 < \lambda < 1 + r_+$.

B. Violation of the fluctuation-dissipation theorem

Having computed both the correlation and response functions for $S(t)$ and $c(t)$ separately, we will now show that these quantities violate the fluctuation-dissipation theorem (FDT) which holds for systems in thermal equilibrium. In Fourier space, the FDT reads (with the Boltzmann constant k_B and the temperature T) [28]

$$\bar\omega\widetilde{\mathcal{C}}(\bar\omega) = 2k_B T\,\mathrm{Im}\,\widetilde{\chi}(\bar\omega), \tag{56}$$

if the correlation function $\widetilde{\mathcal{C}}(\bar\omega)$ and the response function $\widetilde{\chi}(\bar\omega)$ refer to conjugate stimulus and response variables.

To relate to the system considered in this paper, an energy scale ΔU is introduced by writing the ratio of the transition rates (with $c=0$) as $R_+/R_-^0 \equiv r_+ = \exp(-\beta\Delta U)$, where β is the inverse temperature and ΔU is the energy difference between open and closed channel states. Let us now introduce a "field" h which changes the energy gap (analogous to an external magnetic field in the context of magnetic models): $\Delta U \to \Delta U + h$, so that the dimensionless rate r_+ is changed to $r_+' = r_+ e^{-\beta h} \approx r_+(1 - \beta h)$ (where we have assumed that h is small). The relation between the energy change h and the (dimensionless) change in the flipping rate ϕ [which we defined earlier as the stimulus, see Eq. (3)] is therefore, $\phi = -\beta r_+ h$. Using this to transform our (dimensionless) response function $\chi_S(t)$, Eq. (56) can be written dimensionless as

$$\omega\widetilde{\mathcal{C}}_S(\omega) = -2r_+\,\mathrm{Im}\,\widetilde{\chi}_S(\omega), \tag{57}$$

and analogously for c.

In the absence of feedback, we have

$$\widetilde{\mathcal{C}}_S(\omega) = \frac{2r_+}{(1 + r_+)[(1 + r_+)^2 + \omega^2]},$$
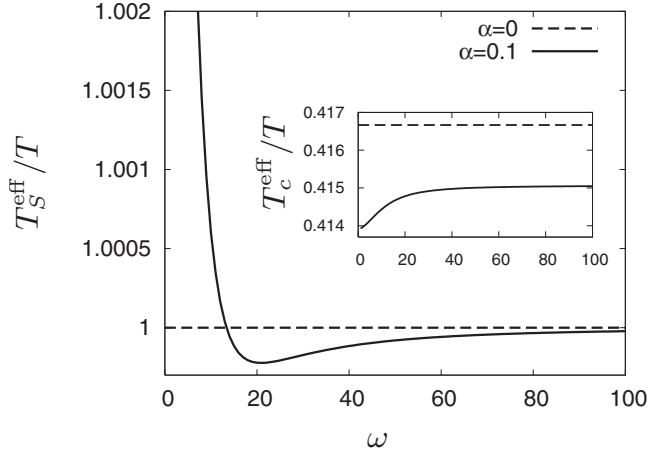
FIG. 6. The ratio T^{eff}/T [defined in Eq. (60); with the Fourier transforms of Eqs. (47), (48), (54), and (55)] of effective and real temperature for the channel state and calcium (inset) is plotted as a function of the frequency ω with and without feedback for $r_+=6$ and $\lambda=5$. Note that the asymptotic limit in the case of calcium is different for the two cases and differs from 1.

$$\widetilde{\chi}_S(\omega) = \frac{1}{(1+r_+)(1+r_++i\omega)}, \qquad (58)$$

from which we find (unsurprisingly) that the FDT holds for $S(t)$. However, for $c(t)$ the analogous results are (with $\alpha=0$)

$$\widetilde{\mathcal{C}}_c(\omega) = \frac{2\lambda^2 r_+}{(1+r_+)[(1+r_+)^2+\omega^2](\lambda^2+\omega^2)},$$

$$\widetilde{\chi}_c(\omega) = \frac{\lambda}{(1+r_+)}\frac{1}{(\lambda+i\omega)(1+r_++i\omega)}, \qquad (59)$$

implying that FDT is violated for $c(t)$, i.e., the dynamics of c cannot be represented by an equilibrium system with the same temperature T that governs the dynamics of S.

In order to characterize this violation quantitatively, it is convenient to introduce an "effective temperature" T^{eff}, defined as the ratio between the left and right hand sides of Eq. (57), multiplied by T [29], as follows:

$$\frac{T_S^{\mathrm{eff}}(\omega)}{T} = -\frac{\omega \widetilde{\mathcal{C}}_S(\omega)}{2r_+ \operatorname{Im}\widetilde{\chi}_S(\omega)} \qquad (60)$$

(analogously for c). T is the real temperature as introduced above. For $\alpha=0$, from Eqs. (58) and (59), we then find that $T_S^{\mathrm{eff}}/T=1$ for S (i.e., FDT is fulfilled), while $T_c^{\mathrm{eff}}/T=\lambda/(1+\lambda+r_+)<1$ for calcium (i.e., FDT is violated). FDT is, however, asymptotically recovered in the limit $\lambda \gg 1+r_+$ [which is the limit where $c(t)$ follows $S(t)$ closely, see Sec. V].

The ratio of effective-to-real temperature, $T^{\mathrm{eff}}(\omega)/T$, is shown in Fig. 6 as a function of ω for both S and c. We see that while the ratio for the channel state approaches unity as $\omega \to \infty$, the corresponding curve for calcium has a different asymptotic limit. The system as a whole is therefore out of
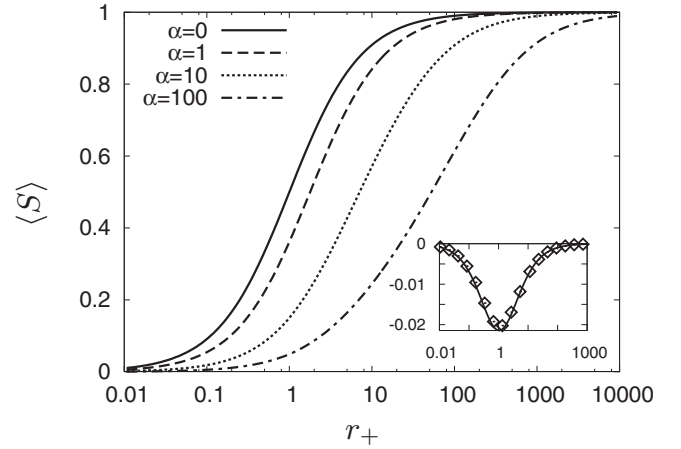

FIG. 7. The numerically obtained open channel fraction $\langle S \rangle$ in the steady state plotted as a function of the opening rate r_+. Inset: Difference between the cases $\alpha=0.1$ and $\alpha=0$. The line represents the term linear in α from the analytical expression in Eq. (40). For the high r_+ values as well as for $\alpha=100$, a smaller time step of $\Delta t=10^{-4}$ was used.

equilibrium already if no feedback is present. With feedback, at least the S variable becomes equilibrated in the limit of high frequencies.

VII. NUMERICAL RESULTS AND DISCUSSION

We carried out numerical simulations in order to verify our analytical results in the weak feedback limit, as well as to study the behavior of the system in the intermediate ($\alpha \simeq 1$) and strong ($\alpha \gg 1$) feedback cases. The dimensionless version of the system described by Eqs. (1)–(3) was simulated using a fixed discrete time step Δt [30,31].

In general, the feedback effects were found to increase in significance with larger λ. However, very high values of λ also tend to make the kinetics of c too closely tied to that of S (see Fig. 4), and for this reason, we performed most of our simulations with the intermediate value $\lambda=5$ (unless otherwise indicated). The weak-feedback ($\alpha=0.1$) case was used for detailed comparison with the analytical results. We observed from the data that the first order perturbation theory works well up to $\alpha \approx 0.2$. Since the difference between the curves for $\alpha=0$ and $\alpha=0.1$ is small, in the following, the $\alpha=0.1$ curve is not shown in the main figures. Instead, the comparison between numerically obtained data points (symbols) and the analytical expressions (lines) is shown in the insets of the figures as differences between the cases with $\alpha=0.1$ and $\alpha=0$. The lines in the main figures connect numerically obtained data points [32].

In Fig. 7, the steady state open fraction $\langle S \rangle$ (which is the same as $\langle c \rangle$) is plotted as a function of the opening rate r_+, for various values of α. This is analogous to a dose-response curve, if the open channel fraction (or, equivalently, the mean Ca^{2+}) is interpreted as the response of the system to an external stimulus that modifies the opening rate of the channels. We observe that feedback shifts the response towards higher r_+ values by closing the channels more often. How-
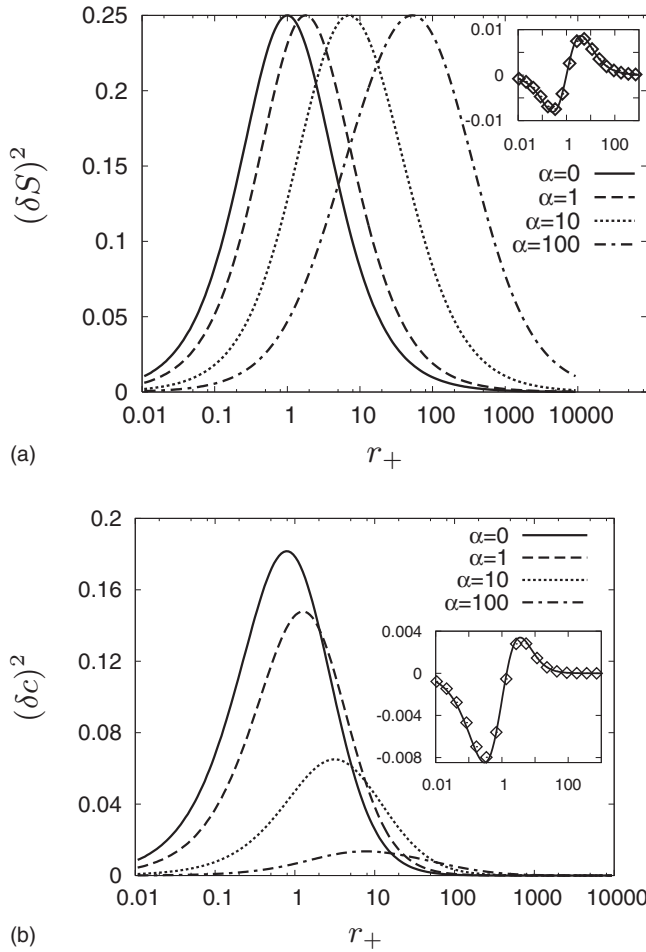
(a)

(b)

FIG. 8. Variance in S (a) and c (b) in the steady state plotted as functions of r_+. Inset: Difference between the cases $\alpha=0.1$ and $\alpha=0$. The line represents the term linear in α from the analytical expressions in Eqs. (51). For the high r_+ values as well as for the case $\alpha=100$ a smaller time step of $\Delta t=10^{-4}$ was used.

ever, the "dynamic range" of sensitivity (e.g., the range of r_+ covered between 5% and 95% of the response) is found to be increased with feedback: the curves become less steep for large α.

In Fig. 8 we show the variances $(\delta S)^2$ and $(\delta c)^2$ of S and c, respectively, in steady state as a function of r_+ for various feedback strengths. The fluctuations follow a bell-shaped curve as a function of r_+, but the maximum shifts towards larger r_+ with increasing feedback. As we remarked in Sec. V, the maximum of the mean squared fluctuations $(\delta S)^2$ is always $\frac{1}{4}$ irrespective of the feedback strength (and occurs when r_+ is comparable to the average closing rate $1+\alpha\langle c\rangle$). For the c fluctuations, however, we find that the fluctuations are generally suppressed by feedback (except at very high r_+). The fluctuations again follow an approximate bell-shaped curve, but the maximum sharply comes down with increasing α and its position shifts to larger r_+. Note also that for $\alpha>0$, the position of the peak for c fluctuations always trails the corresponding point for the channel state.

To investigate how fluctuations affect the precision of signal transduction, we looked at the ratio of the standard de-
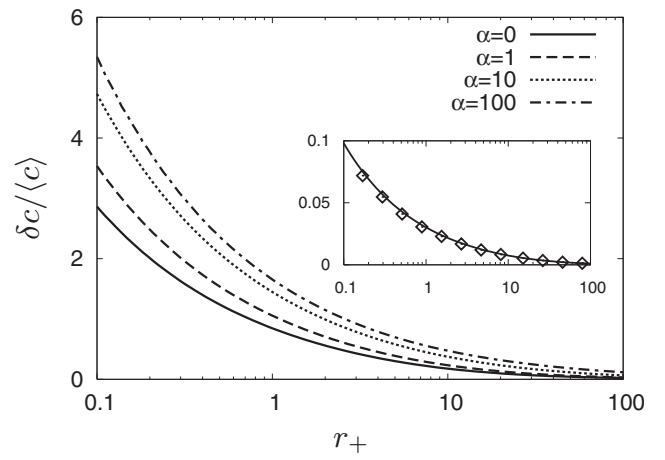

FIG. 9. The coefficient of variation plotted as a function of r_+ for $\lambda=5$. Inset: Difference between the cases $\alpha=0.1$ and $\alpha=0$. The line represents the term linear in α from the analytical expression in Eq. (52). For the high r_+ values as well as for the case $\alpha=100$ a smaller time step of $\Delta t=10^{-4}$ was used.

viation to the mean (i.e., the noise-to-signal ratio in the steady state or the coefficient of variation) for $c(t)$. In Fig. 9 we show $\delta c/\langle c\rangle$ plotted against r_+. For $\lambda=5$, we find that this ratio is a monotonically decreasing function of r_+, independently of feedback. More surprisingly, the ratio itself is enhanced by increasing feedback. Note that for $r_+<0.1$, this ratio is of the order of 10 and is reduced to "acceptable" levels ($\delta c/\langle c\rangle\sim 1$) only for high $r_+\sim 1-10$ depending on the feedback strength. However, the reverse effect is observed when the pumping rate is reduced to $\lambda=0.05$. In this case, for small r_+, the noise-to-signal ratio is reduced by feedback (Fig. 10).

We now turn to time-dependent quantities. Figures 11(a) and 11(b) show the autocorrelation functions for the channel state and calcium, respectively, in the case of strong signal
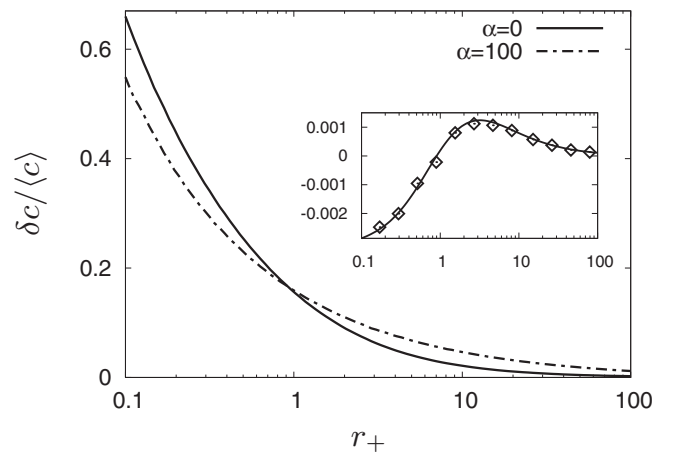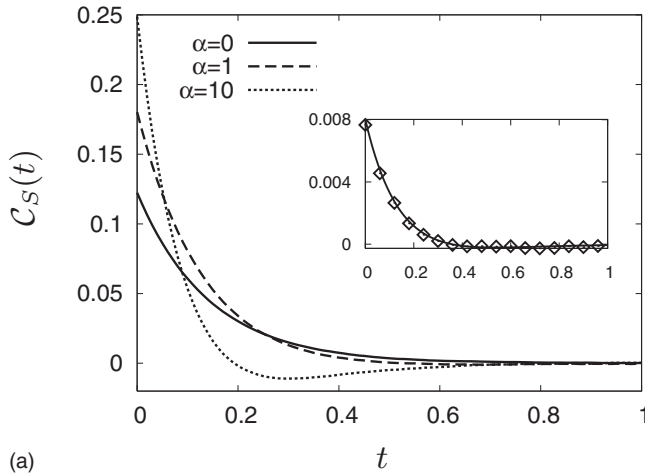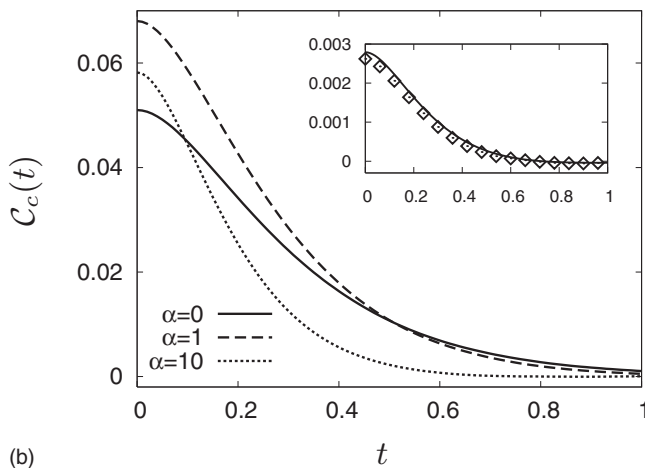

FIG. 10. The coefficient of variation as in Fig. 9, but with $\lambda=0.05$ (only the curves for $\alpha=0$ and 100 are shown for clarity). Note that, in contrast to the previous case, the ratio is reduced with increasing feedback for small r_+, which was also predicted from the first order perturbative correction term in Eq. (52).

(a)

(b)

FIG. 11. Autocorrelation function for $S(t)$ (a) and $c(t)$ (b) in the steady state for $\lambda=5$ and $r_+=6$. Inset: Difference between the cases $\alpha=0.1$ and $\alpha=0$. The line represents the term linear in α from the analytical expressions for $\mathcal{C}_S(t)$ [Eq. (47)] and $\mathcal{C}_c(t)$ [Eq. (48)].

$(r_+=6)$. In general, one notes that the effect of increasing feedback is to reduce the characteristic time scale of decay of the correlations. When the feedback parameter is very large, the channel autocorrelation function briefly becomes negative before vanishing at longer times. This anticorrelation in the channel state may be interpreted physically as the rapid closing of an open channel by the Ca^{2+} which enters through it. In other words, in the presence of feedback, a channel which is open at any point of time has a reduced open probability at subsequent times (compared to the unconditioned mean open probability). By contrast, the autocorrelation function for $c(t)$ for the same parameters decays monotonically with time. In the cases of weak signal ($r_+=0.5$) or high pump rate ($\lambda=50$), both the channel state and calcium autocorrelation functions decay monotonically (data not shown).

In Fig. 12, we plot the power spectral density for calcium and the channel state calculated from the autocorrelation function using Eq. (9), in the presence and absence of feedback. We observe that irrespective of feedback, $P_c(\omega) \sim \omega^{-4}$ and $P_S(\omega) \sim \omega^{-2}$ as $\omega \to \infty$. It may also be noted that $P_S(\omega)$ is nonmonotonic in this plot, and the observed peak is consis-
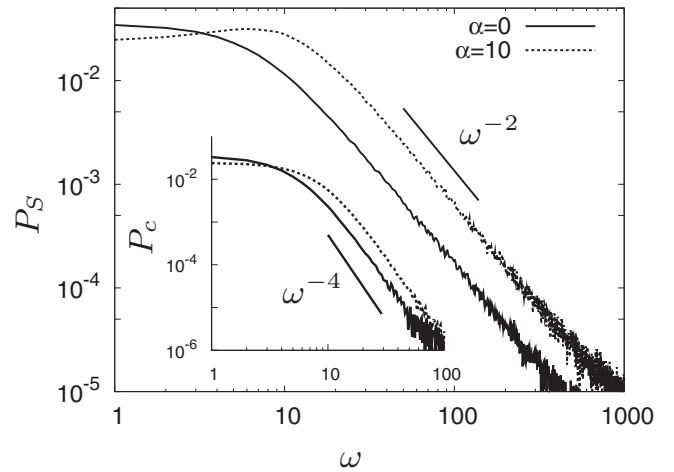

FIG. 12. Power spectral densities for the channel state (main figure) and calcium concentration (inset) are plotted against the angular frequency ω with and without feedback on a logarithmic scale. The parameter values used are $r_+=6$ and $\lambda=5$. The straight lines are guides to the eye. To get results also for high frequencies, a small time step of $\Delta t=10^{-5}$ was used.

tent with the dip in the corresponding autocorrelation function in S [Fig. 11(a)]. Notice also that a similar peak is absent for P_c, which is also consistent with the fact that $\mathcal{C}_c(t)$ is monotonic [Fig. 11(b)]. In a different context, the reduction in noise strength and the shifting of the peak of the power spectrum from low to high frequencies with increasing feedback has also been observed in simulations of a model of an autoregulated gene circuit [33] with negative feedback. An instructive discussion of the general conditions under which feedback can lead to a reduced noise intensity and increased noise bandwidth is given in the Appendix of Ref. [33].

Figure 13 shows the time evolution of the open probability of the channel [Fig. 13(a)] and the mean calcium concentration [Fig. 13(b)] for different values of the feedback parameter α when the channel was initially closed and $c(t=0)=0$. Note that the relaxation to the steady state is monotonic for small α, but for higher α, the response in the channel [Fig. 13(a)] exhibits a maximum, and then settles into the steady state, while the response of c does not show this behavior [Fig. 13(b)].

In Fig. 14, we show the linear response function $\chi_S(T)$ for different values of α. In order to compute the response function numerically, the system was evolved with $r_+=0.5$ until it reached the steady state. Then, r_+ was increased to 0.6 and the response function was calculated using Eq. (10). By definition, the response function shows how a sharply peaked input stimulus [$\phi(t) \sim \delta(t)$] is "transmitted" across the channel. We observe that increasing the feedback reduces the time constant of decay, making the output signal sharper and more similar to the input, when λ is relatively high. This is in agreement with our assertion that high values of λ improve the short-time scale response characteristics of the system. We also confirmed this by studying the effect of λ on the response time when feedback is strong: in this case, reducing λ was found to increase the response time appreciably (for example, when $\alpha=10$, a 50-fold reduction in λ was observed to almost double the response time).
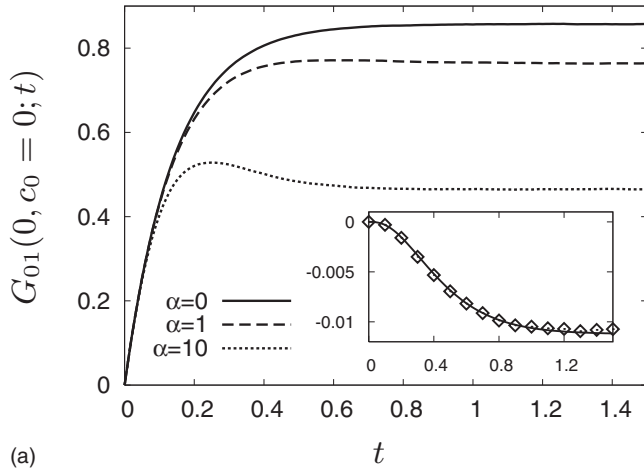
(a)
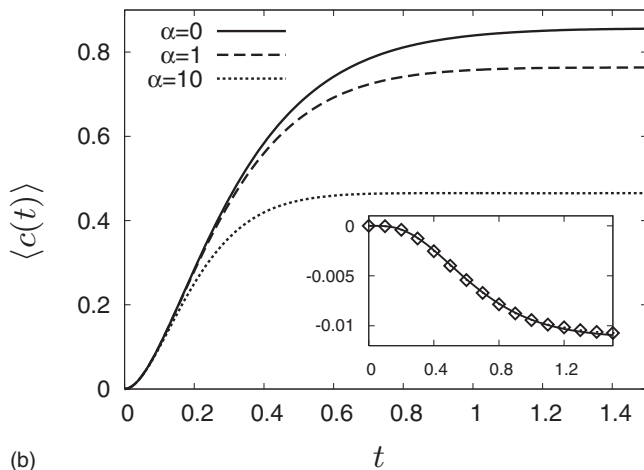
(b)

FIG. 13. Time evolution of the open probability (a) and the mean calcium concentration (b) when the channel starts in the closed state $[S(t=0)=c(t=0)=0]$ for different values of the feedback parameter α. The opening rate is $r_+=6$ and $\lambda=5$. Inset: Difference between the cases $\alpha=0.1$ and $\alpha=0$. The line represents the term linear in α from the analytical expressions Eq. (36) $[G_{01}^{(1)}(0,0,t)]$ and Eq. (5).

We used the channel linear response function derived in Sec. VI to compute the response of the system to a periodic stimulus of the form $\phi(t)=a \sin \omega t$ for 14 different values of ω (Fig. 15). An explicit calculation shows that the linear channel response has the form $\langle S(t)\rangle^\phi - \langle S\rangle = A \sin(\omega t + \theta)$, where both the amplitude A and the phase lag θ are frequency dependent: $A(\omega)=a/(1+r_+)[(1+r_+)^2+\omega^2]^{-1/2}+O(\alpha)$ and $\theta(\omega)=-\frac{\pi}{2}+\arctan[(1+r_+)/\omega]+O(\alpha)$, omitting the $O(\alpha)$ terms for the sake of brevity. The complete expressions [including the first order corrections (to be found at [34])] for A and θ are checked against numerical simulations in the insets of Figs. 15(a) and 15(b). The amplitude is always a decreasing function of the frequency, however, the feedback has the effect of increasing the amplitude of the response relative to the no-feedback case at sufficiently high frequencies. At lower frequencies, the opposite effect is observed: introducing feedback tends to reduce the amplitude of the output, however, the decay as a function of the external frequency is
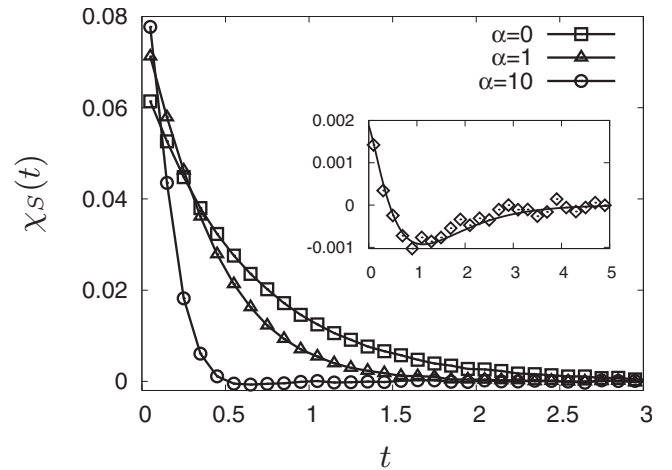

FIG. 14. The linear response function of the system, computed numerically using a step stimulus (see text) and a numerical differentiation for various values of feedback ($\lambda=5$). The points shown are the averages over 10^9 independent runs (symbols are used to indicate the larger error in this calculation—the lines in the main figure are guides to the eye). Inset: The difference between $\alpha=0.1$ and $\alpha=0$ is compared with the analytical expression in Eq. (54) (line).

more gradual. In simple terms, the overall effect of the feedback here is to widen the range of frequencies effectively sensed by the system. The increase in response at large frequencies is consistent with the reduction in the time constant of the linear response function which we noted earlier. At small frequencies, on the other hand, the overall adaptation produced by the negative feedback leads to a drop in the response.

The phase shift of the response decreases monotonically from 0 to $-\frac{\pi}{2}$ as ω is increased, although the change is more gradual when feedback is present. Note that for large α, there is a significant linear regime in the $\theta-\omega$ curve, which means that in this regime, the time delay of the response is effectively independent of the stimulus frequency.

To summarize, numerical simulations provide excellent support for the analytical predictions from the path-integral theory in the weak feedback limit. In addition, we observed qualitatively new features in the autocorrelation function and in the relaxation of the mean open probability to the steady state when feedback is strong. In particular, Figs. 9–11 and 15 are the principal results of this paper, and will be discussed more in the next section in the context of experimental results.

VIII. CONCLUSIONS

In this paper, we studied the stochastic kinetics of a simple autoregulatory signaling module with negative feedback using path-integral techniques and numerical simulations. Within our formalism, all the statistical averages and correlation functions that characterize the long-time kinetics of the system are formally expressed as a power series in the feedback parameter. Explicit expressions were obtained for
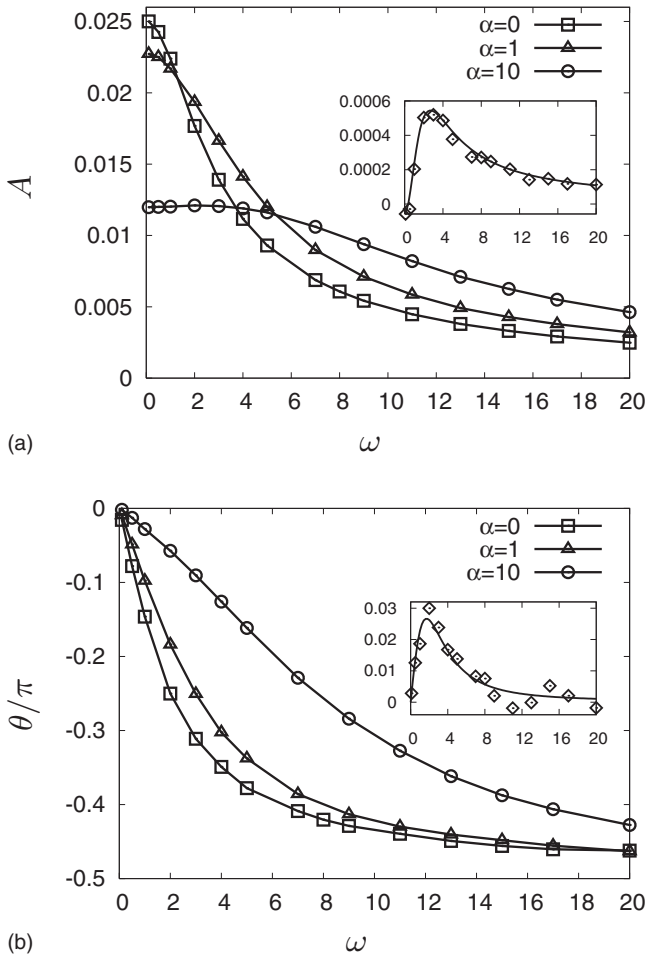
FIG. 15. Amplitude (a) and phase (b) of the response $\langle S(t) \rangle^{\phi}$ to a sinusoidal signal $\phi(t) = a \sin\omega t$ with amplitude $a = 0.1$ and baseline $r_+ = 1$, plotted as a function of stimulus angular frequency ω ($\lambda = 5$). The lines in the main figures are guides to the eye. Inset: Difference between the cases $\alpha = 0.1$ and $\alpha = 0$. The line represents the $O(\alpha)$ correction computed analytically (not shown in text). Note the regime of linear decay of θ versus ω in (b) for small ω, which signifies a constant time delay in the response.

mean values and correlation functions to first order in the feedback parameter. These analytical results were compared to numerical simulations. The simulations were also done in the strong feedback regime beyond the applicability of perturbation theory. In particular, we investigated how the system responds to temporal variations in an external stimulus, and how the feedback regulates this response.

Our principal conclusions from this study may be outlined as follows. We find that, in the context of the ion-channel model, the rate of removal of Ca^{2+} ions, λ, is the single most important control parameter of the model. When λ is large (compared to the intrinsic closing rate for the channel), the short-time scale dynamic response characteristics of the system are improved by negative feedback. In this case, feedback reduces the time scale of decay of the autocorrelation and response functions, and thus extends the response of the system to higher frequencies of input stimulus.

For all parameter values, the negative feedback shifts the range of sensitivity of the system (i.e., the range of stimulus magnitudes for which the response is appreciably nonzero and not saturated) towards stronger stimuli. At the same time, the range of sensitivity gets broader (i.e., the dynamic range is increased) with increasing feedback. While the steady state response to a fixed stimulus is always reduced by the negative feedback, a remarkable effect was seen in the coefficient of variation for the calcium concentration. Increasing the feedback was found to increase this quantity in the large λ regime. For small λ, however, the opposite was seen: the coefficient of variation was reduced with feedback, for sufficiently weak stimuli. In this regime, the negative feedback therefore improves the precision with which one can discriminate among stimuli of different magnitudes based on the system output. Having a small λ, however, was generally found to adversely affect the temporal response characteristics.

Starting from the experimental literature, we have obtained estimates for the dimensionless parameters in our model for the specific case of calcium signaling in olfactory sensory neurons (the corresponding module is shown in the lower part of Fig. 2). The rate of opening of the cyclic-nucleotide-gated channel varies in the range $r_+ \approx 10^{-5}-20$ depending on the strength of the odorant stimulus. The parameter governing the calcium dynamics is $\lambda \approx 20$ and for the feedback parameter we find $\alpha \approx 1-10$ [35]. Note, in particular, that λ is found to have a relatively large value. In the view of our results, this suggests that the calcium-mediated feedback in olfactory transduction evolved so as to improve the temporal response characteristics of the system, rather than to improve the discriminability of weak stimuli.

Our findings are consistent with the results of experimental studies in a variety of sensory systems with calcium-mediated negative feedback. The feedback-induced shift of the range of sensitivity to higher stimulus magnitudes has been demonstrated in olfactory sensory neurons and in cone photoreceptor cells (reviewed in Refs. [36,37]). The temporal characteristic of response was found to be altered in several studies in which the strength of feedback was experimentally manipulated. In Ref. [38], the time course of response to a pulse stimulus was found to be slowed down when the frog olfactory cilium was put in lowered external calcium concentrations (in such conditions, the ion flux J, and therefore the dimensionless coupling α, is decreased). A more pronounced effect of this type was observed in similar experiments for Drosophila photoreceptor cells in Ref. [39]. A marked slowing down of the response to a step stimulus was observed for the newt olfactory cilium in Ref. [40] when the calcium flux J was decreased by changing the holding potential. Fluctuations in the steady state have received less attention in the biological literature. The power spectrum of odorant-induced current fluctuations across the membrane of rat olfactory sensory cilia was studied experimentally by Lowe and Gold [41]. They observed that the tail of the power spectrum decays with an effective exponent in the range 2.3–2.5, which is suggestive of a crossover between ω^{-2} and ω^{-4} decay. In this case, however, the dynamics of the cAMP module (shown in the upper part of Fig. 2) should be taken into account in the theoretical treatment, as fluctuations in cAMP give an important contribution to the variability of the response [41].

We are currently in the process of extending this study to include spatial effects. In particular, in olfactory sensory neurons, the Ca^{2+} ion channels are spatially distributed along long and thin cellular compartments called cilia. The feedback studied in the present manuscript coupled with calcium diffusion inside the cilium can give rise to nontrivial spatial correlations between the channels, and it will be interesting to study how the spatial coupling affects the overall kinetics of the system.

APPENDIX A: CALCULATION OF INTEGRALS I_0, I_1, AND I_2

1. Generalized convolution theorem

The following general result is very useful in performing many calculations using the path-integral technique. If $g(t) = \int_0^t f_1(t_1) \int_0^{t-t_1} f_2(t_2) \cdots \int_0^{t-\cdots-t_{n-1}} f_n(t_n)$, then its Laplace transform $\tilde{g}(s) = \int_0^\infty g(t) e^{-st} dt$ is given by

$$\tilde{g}(s) = \frac{1}{s} \prod_{i=1}^n \tilde{f}_i(s). \tag{A1}$$

This result is proved in a straightforward way by repeated application of the standard convolution theorem of Laplace transforms.

2. Calculation of I_0

The integral I_0 is relatively easy to compute. The Laplace transform $\tilde{I}_0(s)$ can be written easily from the definition of the integral in Eq. (34) and using the above theorem as follows:

$$\tilde{I}_0(s;m) = s^{-(m+1)}(s+1-r_+)^{-m}. \tag{A2}$$

3. Calculation of I_1

In order to calculate the integrals I_1 and I_2, it is necessary to express $c(t)$ in terms of the time interval variables using Eq. (5). The explicit relations are

$$c(\tau) = 1 - e^{-\lambda(\tau-\tau_1)} \quad \text{for } \tau_1 \leqslant \tau \leqslant \tau_2,$$

$$c(\tau) = 1 + e^{-\lambda\tau}(e^{\lambda\tau_2} - e^{\lambda\tau_1} + \cdots + e^{\lambda\tau_{j-1}} - e^{\lambda\tau_j})$$

$$\text{for } \tau_j \leqslant \tau \leqslant \tau_{j+1} \quad \text{with odd } j \geqslant 3. \tag{A3}$$

From that it follows

$$c(\tau_i) = \sum_{j=1}^{i-1}{}''(e^{-\lambda(\tau_i-\tau_{j+1})} - e^{-\lambda(\tau_i-\tau_j)}) \quad \text{for even } i \geqslant 2. \tag{A4}$$

Using Eq. (A4) in Eq. (34), we write $I_1 = g_1 - g_2$, with

$$g_1(0,t;m) = \sum_{i=2}^{2m}{}' \sum_{j=1}^{i-1}{}'' \int \mathcal{DT}$$

$$\times \exp\left(-\left[(1-r_+)\sum_{k=1}^m t_k' + \lambda(\tau_i - \tau_{j+1})\right]\right), \tag{A5}$$

and

$$g_2(0,t;m) = \sum_{i=2}^{2m}{}' \sum_{j=1}^{i-1}{}'' \int \mathcal{DT}$$

$$\times \exp\left(-\left[(1-r_+)\sum_{k=1}^m t_k' + \lambda(\tau_i - \tau_j)\right]\right). \tag{A6}$$

Note that when $j \leqslant i-3$, $\tau_i - \tau_{j+1} = \sum_{(j+3)/2}^{i/2}(t_k' + t_k)$ and is zero when $j = i-1$. Let us therefore split the second sum, and treat these cases separately. In order to compute the Laplace transforms, we use the theorem in Eq. (A1). It is now straightforward to write the Laplace transform of g_1 in Eq. (A5) using this theorem. The result is

$$\tilde{g}_1(s) = ms^{-(m+1)}$$

$$\times (s+1-r_+)^{-m} + s^{-(m+1)}(s+1$$

$$- r_+)^{-m} \sum_{i=4}^{2m}{}' y^{i/2} \sum_{j=1}^{i-3}{}'' y^{-(j+1)/2}, \tag{A7}$$

where we have defined $y = s(s+\lambda)^{-1}(s+1-r_+)(s+1-r_+ +\lambda)^{-1} < 1$. The double geometric sum in Eq. (A7) turns out to be $y(1-y)^{-1}[m+(1-y)^{-1}(y^m-1)]$, which gives

$$\tilde{g}_1(s) = s^{-(m+1)}(s+1-r_+)^{-m} \frac{1}{1-y}\left(m + \frac{y}{1-y}(y^m-1)\right). \tag{A8}$$

Calculation of g_2 also proceeds along similar lines. After some straightforward algebra, we find that

$$\tilde{g}_2(s) = s^{-(m+1)}(s+1-r_+)^{-m} \frac{s+1-r_+}{s+1-r_+ +\lambda}$$

$$\times \left(m + \sum_{i=2}^{2m}{}' y^{i/2} \sum_{l=1}^{i/2-1} y^{-l}\right). \tag{A9}$$

The double sum is easily shown to be equal to $y(1-y)^{-1}[m +(1-y)^{-1}(y^m-1)]$, and this gives

$$\tilde{g}_2(s) = s^{-(m+1)}(s+1-r_+)^{-m}\frac{s+1-r_+}{s+1-r_++\lambda}$$

$$\times\frac{1}{1-y}\left(m+\frac{y}{1-y}(y^m-1)\right). \qquad (A10)$$

After putting together Eqs. (A8) and (A10), we arrive at

$$\tilde{I}_1(s;m) = s^{-(m+1)}(s+1-r_+)^{-m}\frac{s+\lambda}{2s+1-r_++\lambda}$$

$$\times\left(m+\frac{y}{1-y}(y^m-1)\right). \qquad (A11)$$

4. Calculation of I_2

For I_2, the following integral is needed [obtained using Eqs. (A3)]:

$$\int_{\tau_j}^{\tau_{j+1}} c(\tau)d\tau = t'_{(j+1)/2} + \frac{1}{\lambda}(e^{-\lambda\tau_j}-e^{-\lambda\tau_{j+1}})$$

$$\times\left(\sum_{k=2}^{j-1}{}' e^{\lambda\tau_k}-\sum_{l=1}^{j}{}'' e^{\lambda\tau_l}\right) \qquad (A12)$$

for odd $j\geq 1$.

The integral I_2 may be expressed in the form

$$I_2(0,t;m) = h_0 + h_1 + \frac{1}{\lambda}(h_2+h_3-h_4-h_5), \qquad (A13)$$

where

$$h_0 = \int \mathcal{D}T\exp\left[(r_+-1)\sum_{k=1}^m t'_k\right]\int_{\tau_1}^{\tau_2} c(\tau)d\tau,$$

$$h_1 = \sum_{j=3}^{2m-1}{}''\int \mathcal{D}T\exp\left[(r_+-1)\sum_{k=1}^m t'_k\right]t'_{(j+1)/2},$$

$$h_2 = \sum_{j=3}^{2m-1}{}''\sum_{k=2}^{j-1}{}'\int \mathcal{D}T\exp\left[(r_+-1)\sum_{l=1}^m t'_l+\lambda(\tau_j-\tau_k)\right],$$

$$h_3 = \sum_{j=3}^{2m-1}{}''\sum_{l=1}^{j}{}''\int \mathcal{D}T\exp\left[(r_+-1)\sum_{k=1}^m t'_k+\lambda(\tau_{j+1}-\tau_l)\right],$$

$$h_4 = \sum_{j=3}^{2m-1}{}''\sum_{l=1}^{j}{}''\int \mathcal{D}T\exp\left[(r_+-1)\sum_{k=1}^m t'_k+\lambda(\tau_j-\tau_l)\right],$$

$$h_5 = \sum_{j=3}^{2m-1}{}''\sum_{k=2}^{j-1}{}'\int \mathcal{D}T\exp\left[(r_+-1)\sum_{l=1}^m t'_l+\lambda(\tau_{j+1}-\tau_k)\right]. \qquad (A14)$$

Obviously, h_0 represents $j=1$ in the sum in Eq. (34), and hence includes all possible contributions from $m=1$. The rest of the terms therefore always have $m\geq 2$. The Laplace trans-

forms for h_0 and h_1 are straightforward, and one may easily verify that

$$\tilde{h}_0(s) = s^{-(m+1)}(s+1-r_+)^{-m}\left(\frac{1}{s+1-r_+}-\frac{1}{s+1-r_++\lambda}\right),$$

$$\tilde{h}_1(s) = s^{-(m+1)}(s+1-r_+)^{-m}\frac{m-1}{s+1-r_+}, \quad m\geq 2, \qquad (A15)$$

so that

$$\tilde{h}_0+\tilde{h}_1 = s^{-(m+1)}(s+1-r_+)^{-m}\left(\frac{m}{s+1-r_+}-\frac{1}{s+1-r_++\lambda}\right) \qquad (A16)$$

for $m\geq 2$. We omit further details of computation of h_2, h_3, h_4, and h_5, which involves straightforward, but somewhat tedious algebra. The results are (for $m\geq 2$)

$$\tilde{h}_2(s) = s^{-(m+1)}(s+1-r_+)^{-m}$$

$$\times\left(m+\frac{y^m-1}{1-y}\right)\frac{s}{\lambda}\frac{s+1-r_++\lambda}{2s+1-r_++\lambda},$$

$$\tilde{h}_3(s) = s^{-(m+1)}(s+1-r_+)^{-m}\left(m+\frac{y(y^m-1)}{1-y}-(1-y)\right)$$

$$\times\left(\frac{s}{\lambda}+1\right)\frac{s+1-r_+}{2s+1-r_++\lambda},$$

$$\tilde{h}_4(s) = s^{-(m+1)}(s+1-r_+)^{-m}\left(m+\frac{y(y^m-1)}{1-y}-(1-y)\right)$$

$$\times\left(\frac{s}{\lambda}+1\right)\frac{s+1-r_++\lambda}{2s+1-r_++\lambda},$$

$$\tilde{h}_5(s) = s^{-(m+1)}(s+1-r_+)^{-m}$$

$$\times\left(m+\frac{y^m-1}{1-y}\right)\frac{s}{\lambda}\frac{s+1-r_+}{2s+1-r_++\lambda}. \qquad (A17)$$

After putting together all the terms, we show that

$$\tilde{I}_2(s;1) = s^{-2}(s+1-r_+)^{-1}\left(\frac{1}{s+1-r_+}-\frac{1}{s+1-r_++\lambda}\right), \qquad (A18)$$

and for $m\geq 2$,

$$\tilde{I}_2(s;m) = s^{-(m+1)}(s+1-r_+)^{-m}$$

$$\times\left(\frac{m(s+\lambda)}{(s+1-r_+)(2s+1-r_++\lambda)}\right.$$

$$\left.+\frac{y^m-1}{1-y}\frac{s}{(s+1-r_++\lambda)(2s+1-r_++\lambda)}\right). \qquad (A19)$$

APPENDIX B: RELATION BETWEEN G_{11} AND G_{00} FOR $\alpha \neq 0$

In order to prove Eq. (37) to be valid up to $O(\alpha)$, we first calculate the functions $f_1(t)$ and $f_2(t)$. As in Eq. (31), in Eq. (39) $c'f_1(t)$ and $c'f_2(t)$ are the $O(\alpha)$ terms in $G_{01}(0,c';t)$ and $G_{11}(0,c';t)$, respectively, when the channel does not allow entry of ions. The solution is obtained by solving the corresponding rate equations with the time-dependent rate $r_-(t) = 1 + \alpha c' e^{-\lambda t}$. The results are

$$f_1(t) = -f(t),$$

$$f_2(t) = -\frac{1}{\lambda}\left(\frac{1-\lambda}{1+r_+ - \lambda}e^{-(1+r_+)t} - \frac{1}{1+r_+}e^{-(1+r_++\lambda)t}\right.$$
$$\left. + \frac{\lambda r_+}{(1+r_+)(1+r_+-\lambda)}e^{-\lambda t}\right). \quad (B1)$$

Instead of Eq. (38), we now write a relation between the full propagators Π with $0 \leq t' \leq t$ as follows:

$$G_{01}(0,0;t) = \sum_j \int_0^1 dc' \int_0^1 dc \Pi_{0j}(0,0;t',c')\Pi_{j1}(t',c';t,c)$$
$$= \int_0^1 dc' \Pi_{00}(0,0;t',c')G_{01}(t',c';t)$$
$$+ \int_0^1 dc' \Pi_{01}(0,0;t',c')G_{11}(t',c';t). \quad (B2)$$

After substituting Eq. (39) into Eq. (B2), we find that

$$G_{01}(0,c_0=0;t) = G_{00}(0,c_0=0;t')G_{01}(t',c'=0;t)$$
$$+ G_{01}(0,c_0=0;t')G_{11}(t',c'=0;t)$$
$$+ \alpha[f_1(t-t')\langle c'(t')\rangle_0$$
$$+ f_2(t-t')\langle c'(t')\rangle_1] + O(\alpha^2), \quad (B3)$$

where $\langle c'(t')\rangle_0$ and $\langle c'(t')\rangle_1$ were defined in Eq. (13). Let us now take the limit of $t' \to 0$ as in the case without feedback, and express the Green's function G_{11} in terms of G_{00}. The result, to $O(\alpha)$ is

$$G_{11}(0,c_0=0;t) = 1 - G_{00}(0,0;t)$$
$$+ \frac{1}{\partial_t G_{00}(0,0;t)|_{t=0}}[\partial_t G_{00}(0,0;t)$$
$$- \alpha(f_1(t)\partial_{t'}\langle c'(t')\rangle_0|_{t'=0} + f_2(t)\partial_{t'}\langle c'(t')\rangle_1|_{t'=0})]. \quad (B4)$$

It is easy to see now that both the time derivatives of $\langle c'(t')\rangle_{0/1}$ in the previous equation vanish, simply because they are defined in Eq. (13) with an initial condition $c(0)=0$ *by construction*. This is easily seen by first solving Eq. (5) to find $\langle c(t)\rangle$ to order $\alpha=0$, and the result is

$$\langle c(t)\rangle = \frac{r_+}{(1+r_+)}\left(1 - \frac{1}{1+r_+-\lambda}[(1+r_+)e^{-\lambda t} - \lambda e^{-(1+r_+)t}]\right)$$
$$+ O(\alpha), \quad (B5)$$

whose time derivative vanishes at $t=0$. But, since $\langle c(t)\rangle = \langle c(t)\rangle_0 + \langle c(t)\rangle_1$ and since $\partial_t\langle c(t)\rangle_{0/1}|_{t=0} \gtrless 0$, it follows that $\partial_t\langle c(t)\rangle_{0/1}|_{t=0}=0$ in Eq. (B4) and this leads to Eq. (37).

APPENDIX C: CALCULATION OF $\langle c\rangle_0$ AND $\langle c\rangle_1$

In this appendix, we compute $\langle c(t)\rangle_0$, whose long-time limit gives $\langle c\rangle_0$. Note that, in accordance with Eq. (B3), this quantity needs to be computed only to the zeroth order in α. This can be done using the probability functional $\mathcal{P}_{00}$ from Eq. (23). We therefore define

$$\langle c(t)\rangle_0 = \sum_{m=0}^{\infty} \int \mathcal{D}T \, \mathcal{P}_{00}[0,t;\{t_i\},\{t_i'\};2m]c(t), \quad (C1)$$

where $c(t) = e^{-\lambda t}\sum_{j=1}^{''2m-1}(e^{\lambda \tau_{j+1}} - e^{\lambda \tau_j})$ from Eq. (5). Further calculations are done with the aid of Laplace transforms and using the generalized convolution theorem [Eq. (A1)]. We omit further details, and simply give the final result for the Laplace transform $\langle \tilde{c}(s)\rangle_0$ as follows:

$$\langle \tilde{c}(s)\rangle_0 = \frac{r_+\lambda}{s(s+\lambda)(s+1+r_+)(s+1+r_++\lambda)}. \quad (C2)$$

The steady state value is obtained after inversion $s \to t$ and taking the limit $t \to \infty$ and is easily found to be

$$\langle c\rangle_0 = \frac{r_+}{1+r_+}\frac{1}{1+r_++\lambda}, \quad (C3)$$

from which we also find

$$\langle c\rangle_1 = \langle c\rangle - \langle c\rangle_0 = \frac{r_+}{1+r_+}\frac{r_++\lambda}{1+r_++\lambda}. \quad (C4)$$

APPENDIX D: LIST OF COEFFICIENTS IN THE FIRST ORDER TERMS

1. Correlation functions

$$B_1 = -\frac{r_+}{(1+r_+)^3(1+r_+-\lambda)^2\lambda(1+r_++\lambda)}$$
$$\times[-(\lambda-1)r_+^4 - (\lambda-1)(2-\lambda)r_+^3$$
$$+ \lambda(\lambda^2 - 2\lambda - 1)r_+^2 + (-\lambda^4 + \lambda^3 - 3\lambda^2$$
$$+ 3\lambda - 2)r_+ + (\lambda-1)^2(\lambda+1)(\lambda-1)],$$

$$C_1 = -\frac{2r_+^2\lambda}{(1+r_+)^2(1+r_+-\lambda)^2(1+r_++\lambda)},$$

$$D_1 = \frac{r_+(r_+^2-1)}{(1+r_+)^3\lambda(1+r_++\lambda)},$$

$$E_1 = \frac{r_+(\lambda - 1)}{(1 + r_+)^2(1 + r_+ - \lambda)},$$

$$\begin{aligned} B_2 = {} & -\frac{r_+\lambda}{(1 + r_+)^3(1 + r_+ - \lambda)^3(1 + r_+ + \lambda)^2}[(\lambda - 1)r_+^4 + (\lambda - 1) \\ & \times (2 - \lambda)r_+^3 - \lambda(\lambda^2 - 4\lambda + 1)r_+^2 + (\lambda^4 - \lambda^3 + 7\lambda^2 - 7\lambda \\ & + 2)r_+ - (\lambda - 1)(\lambda^3 - \lambda^2 - 3\lambda + 1)], \end{aligned}$$

$$\begin{aligned} C_2 = {} & \frac{r_+\lambda}{(1 + r_+)^3(1 + r_+ - \lambda)^3(1 + r_+ + \lambda)^2(1 + r_+ + 2\lambda)} \\ & \times [r_+^6 + (1 + \lambda)r_+^5 - (3\lambda^2 - 5\lambda + 6)r_+^4 + (-\lambda^3 + 4\lambda^2 + 6\lambda \\ & - 14)r_+^3 + (2\lambda^4 + \lambda^3 + 18\lambda^2 - 2\lambda - 11)r_+^2 + (\lambda^4 + 3\lambda^3 \\ & + 12\lambda^2 - 7\lambda - 3)r_+ + \lambda(\lambda^3 + \lambda^2 + \lambda - 3)], \end{aligned}$$

$$D_2 = -\frac{r_+\lambda(r_+ - 1)}{(1 + r_+)^3(1 + r_+ + \lambda)(1 + r_+ + 2\lambda)},$$

$$\begin{aligned} E_2 = {} & -\frac{r_+\lambda^2(\lambda - 1)}{(1 + r_+)^3(1 + r_+ - \lambda)^3(1 + r_+ + \lambda)^2} \\ & \times [r_+^3 + 3r_+^2 + (3 - \lambda^2)r_+ - (\lambda^2 - 1)], \end{aligned}$$

$$F_2 = -\frac{r_+^2\lambda^2}{(1 + r_+)^2(1 + r_+ - \lambda)^2(1 + r_+ + \lambda)}.$$

2. Response functions

$$\begin{aligned} B_3 = {} & -\frac{1}{\lambda(1 + r_+)^2(1 + r_+ - \lambda)^2}[-(\lambda - 1)r_+^3 + (2\lambda^2 - 4\lambda \\ & + 1)r_+^2 + (-\lambda^3 + 2\lambda^2 - \lambda - 1)r_+ - (\lambda - 1)^2], \end{aligned}$$

$$C_3 = -\frac{r_+\lambda}{(1 + r_+)^2(1 + r_+ - \lambda)^2},$$

$$D_3 = \frac{r_+^2 - \lambda - 1}{(1 + r_+)^2\lambda(1 + r_+ + \lambda)},$$

$$E_3 = \frac{\lambda - 1}{(1 + r_+)(1 + r_+ - \lambda)},$$

$$\begin{aligned} B_4 = {} & -\frac{1}{(1 + r_+)^2(1 + r_+ - \lambda)^3}\{1 + \lambda(2\lambda - 3) + r_+[1 + \lambda^2(\lambda \\ & - 1)] - r_+^2[1 + 2\lambda(\lambda - 2)] + r_+^3(\lambda - 1)\}, \end{aligned}$$

$$\begin{aligned} C_4 = {} & \frac{\lambda}{(1 + r_+)^3(1 + r_+ - \lambda)^3(1 + r_+ + \lambda)} \\ & \times \{\lambda^3(1 + r_+ + r_+^2) - \lambda^2 r_+(1 + r_+)^2 - \lambda(1 + r_+)^2 \\ & \times [1 + r_+(r_+ - 5)] + r_+(r_+ - 1)(1 + r_+)^3\}, \end{aligned}$$

$$D_4 = -\frac{r_+^2 - \lambda - 1}{(1 + r_+)^3(1 + r_+ + \lambda)},$$

$$E_4 = -\frac{\lambda(\lambda - 1)}{(1 + r_+)(1 + r_+ - \lambda)^2},$$

$$F_4 = -\frac{r_+\lambda^2}{(1 + r_+)^2(1 + r_+ - \lambda)^2}.$$

[1] H. C. Berg and E. M. Purcell, Biophys. J. **20**, 193 (1977).
[2] W. Bialek, Annu. Rev. Biophys. Biophys. Chem. **16**, 455 (1987).
[3] C. V. Rao, D. M. Wolf, and A. P. Arkin, Nature (London) **420**, 231 (2002).
[4] M. Falcke, L. S. Tsimring, and H. Levine, Phys. Rev. E **62**, 2636 (2000).
[5] T. B. Kepler and T. C. Elston, Biophys. J. **81**, 3116 (2001).
[6] P. S. Swain, M. B. Elowitz, and E. D. Siggia, Proc. Natl. Acad. Sci. U.S.A. **99**, 12795 (2002).
[7] J. Paulsson, Nature (London) **427**, 415 (2004).
[8] U. S. Bhalla, Biophys. J. **87**, 733 (2004).
[9] B. Mazzag, C. J. Tignanelli, and G. D. Smith, J. Theor. Biol. **235**, 121 (2005).
[10] W. Bialek and S. Setayeshgar, Proc. Natl. Acad. Sci. U.S.A. **102**, 10040 (2005).
[11] I. Goychuk, P. Hänggi, J. L. Vega, and S. Miret-Artes, Phys. Rev. E **71**, 061906 (2005).
[12] A. Arkin, J. Ross, and H. H. McAdams, Genetics **149**, 1633 (1998).
[13] J. M. Vilar, H. Y. Kueh, N. Barkai, and S. Leibler, Proc. Natl. Acad. Sci. U.S.A. **99**, 5988 (2002).
[14] C. McNeilage, E. N. Ivanov, P. R. Stockwell, and J. H. Searls, Proceedings of the IEEE 1998 International Frequency Control Symposium (IEEE Press, New York, 1998), 146 (1998).
[15] L. H. Hartwell, J. J. Hopfield, S. Leibler, and A. W. Murray, Nature (London) **402**, C47 (1999).
[16] E. Yeger-Lotem, S. Sattath, N. Kashtan, S. Itzkovitz, R. Milo, R. Y. Pinter, U. Alon, and H. Margalit, Proc. Natl. Acad. Sci. U.S.A. **101**, 5934 (2004).
[17] P. B. Detwiler, S. Ramanathan, A. Sengupta, and B. Shraiman, Biophys. J. **79**, 2801 (2000).
[18] S. Firestein, Nature (London) **413**, 211 (2001).
[19] D. Schild and D. Restrepo, Physiol. Rev. **78**, 429 (1998).
[20] N. G. van Kampen, *Stochastic Processes in Physics and Chemistry* (North-Holland, Amsterdam, 1992).
[21] M. Thattai and A. van Oudenaarden, Biophys. J. **82**, 2943 (2002).

[22] I. Goychuk and P. Hänggi, Phys. Rev. E **61**, 4272 (2000).

[23] F. Zufall and T. Leinders-Zufall, Chem. Senses **25**, 473 (2000).

[24] J. Bradley, D. Reuter, and S. Frings, Science **294**, 2176 (2001).

[25] J. Reidl, P. Borowski, A. Sensse, J. Starke, M. Zapotocky, and M. Eiswirth, Biophys. J. **90**, 1147 (2006).

[26] Higher order correlation functions can be expressed in the path integral representation as $\langle S(t_0)\cdots S(t_{n-1})\rangle = \Sigma_{m_1,\ldots,m_n=0}^{\infty}\int\mathcal{D}\{\tau\}_1\mathcal{P}_{01}[-\infty,t_0;\{\tau\}_1;0;2m_1+1]\int\mathcal{D}\{\tau\}_2\mathcal{P}_{11}[t_0,t_1;\{\tau\}_2;c_0;2m_2]\cdots\int\mathcal{D}\{\tau\}_n\mathcal{P}_{11}[t_{n-2},t_{n-1};\{\tau\}_n;c_{n-2};2m_n]$. In the presence of a feedback, the weights $\mathcal{P}_{ij}[t_0,t;\{\tau_k\}_{k=1}^{N};c_0;N]$ are functions of the concentration c_0 at time t_0. Since for any realization $S(t)$, the function $c(t)$ follows according to Eq. (5), the values $c_k=c(t_k)$ are nontrivial. As a consequence, correlation functions of order larger than two cannot be written as simple products of propagators.

[27] Putting in the coefficients from Appendix D shows that the terms $\sim\omega^{-2}$ cancel also for $\alpha\neq 0$.

[28] L. D. Landau and E. M. Lifshitz, *Statistical Physics*, Part 1 (Pergamon Press, New York, 1997).

[29] P. Martin, A. J. Hudspeth, and F. Jülicher, Proc. Natl. Acad. Sci. U.S.A. **98**, 14380 (2001).

[30] The time step was chosen to be much smaller than all the relevant time scales: $\Delta t\ll\min\{\frac{1}{r_+},\frac{1}{1+\alpha},\frac{1}{\lambda}\}$. The kinetics of the (dimensionless) calcium concentration is computed using a simple Euler forward step algorithm. (Unless otherwise indicated, we used $\Delta t=10^{-3}$ and the curves presented are averages over 10^6 independent runs.) Feedback strengths $\alpha=0$, 0.1, 1, 10, and 100 were used, and r_+ values were chosen from the range [0.01, 10000].

[31] In principle, a Gillespie-type algorithm [42] could be used. Its implementation would, however, require numerically inverting the dwelling time distribution $P_1(t)=\exp\{-\frac{1}{\lambda}[\alpha(c(\tau_j)-1)](1-e^{-\lambda t})-(1+\alpha)t\}$ for the open state for each value of c (see also [9]). It is not clear, if this approach would decrease computer time compared to the fixed time step algorithm.

[32] The data points in the main figures (many hundreds in the plots over time, approximately 200 in the plots over r_+) are equally spaced on the linear or logarithmic scale. Through variation of Δt and the number of independent runs used to calculate the averages, it was checked, that the systematic error due to time discretization and restricted sampling size is in the range of line thickness. In the insets as well as in the main figures of Figs. 14 and 15, this error is smaller than or comparable to the symbol size.

[33] M. L. Simpson, C. D. Cox, and G. S. Sayler, Proc. Natl. Acad. Sci. U.S.A. **100**, 4551 (2003).

[34] P. Borowski, dissertation, TU Dresden, 2006.

[35] To obtain these estimates, we view the olfactory cilium as consisting of a series of cylindrical segments, each containing one cyclic-nucleotide-gated (CNG) channel. On the time scales of interest, we neglect calcium diffusion between neighboring segments. We estimate the parameter values in each segment as follows: $J\approx 1.3\times 10^{-19}$ mol s^{-1} [43]; $V\approx 6\times 10^{-24}$ m^3 (calculated from the density of CNG channels and the geometry of the cilium as cited in [25], assuming a homogeneous distribution of channels); $\bar{\lambda}\approx 10^4$ s^{-1} (calculated from a Taylor expansion of the calcium-extrusion term used in the deterministic model of Ref. [25]); $R_-^0\approx 500$ s^{-1} [from single channel measurements with weak stimulus and low calcium (e.g., [44,45])]; $R_+\approx 5\times 10^{-3}$–$10^4$ s^{-1} (based on an open probability of 10^{-5} if no stimulus is present to 0.95 for full activation [46]); $\bar{\alpha}\approx 3\times 10^8$–$2\times 10^9$ s^{-1} M^{-1} [based on data in the figures of Refs. [47] (lower estimate) and [48] (upper estimate)].

[36] J. Bradley, J. Reisert, and S. Frings, Curr. Opin. Neurobiol. **15**, 343 (2005).

[37] S. Pifferi, A. Boccaccio, and A. Menini, FEBS Lett. **580**, 2853 (2006).

[38] V. Bhandawat, J. Reisert, and K. W. Yau, Science **308**, 1931 (2005).

[39] S. R. Henderson, H. Reuss, and R. C. Hardie, J. Physiol. (London) **524**, 179 (2000).

[40] H. Takeuchi and T. Kurahashi, J. Physiol. (London) **541**, 825 (2002).

[41] G. Lowe and G. H. Gold, Proc. Natl. Acad. Sci. U.S.A. **92**, 7864 (1995).

[42] D. T. Gillespie, J. Phys. Chem. **81**, 2340 (1977).

[43] J. Reisert, P. J. Bauer, K. W. Yau, and S. Frings, J. Gen. Physiol. **122**, 349 (2003).

[44] M. Ruiz and J. W. Karpen, J. Gen. Physiol. **113**, 873 (1999).

[45] P. Gavazzo, C. Picco, E. Eismann, U. B. Kaupp, and A. Menini, J. Gen. Physiol. **116**, 311 (2000).

[46] U. Kaupp and R. Seifert, Physiol. Rev. **82**, 769 (2002).

[47] S. J. Kleene, J. Neurophysiol. **81**, 2675 (1999).

[48] J. Bradley, W. Bönigk, K. W. Yau, and S. Frings, Nat. Neurosci. **7**, 705 (2004).